REPORT DOCUMENTATION PAGE

Form Approved
OMB No. 0704-0188

1. REPORT DATE *(DD-MM-YYYY)*	2. REPORT DATE	3. DATES COVERED *(From - To)*
24-04-2003	Final	Mar 1998-Dec 2001

4. TITLE AND SUBTITLE
ACTIVE CONTROL OF HIGH SPEED JET FLAMES USING COUNTERFLOW

5a. CONTRACT NUMBER

5b. GRANT NUMBER
N00014-98-1-0424

5c. PROGRAM ELEMENT NUMBER

6. AUTHOR(S)
Krothapalli, Anjaneyulu
Lourenco, Luiz M.
Koc-Alkislar, Esin

5d. PROJECT NUMBER

5e. TASK NUMBER

5f. WORK UNIT NUMBER

7. PERFORMING ORGANIZATION NAME(S) AND ADDRESS(ES)
Florida State University
118 N.Woodward Ave.
Tallahassee FL32306-4166

8. PERFORMING ORGANIZATION REPORT NUMBER
FMRL-03-02

9. SPONSORING/MONITORING AGENCY NAME(S) AND ADDRESS(ES)
Office of Naval research
100 Alabama St. NW Suit 4R15
Atlanta, GA 30303-3104

10. SPONSOR/MONITOR'S ACRONYM(S)
ONR

11. SPONSORING/MONITORING AGENCY REPORT NUMBER

12. DISTRIBUTION AVAILABILITY STATEMENT
Approved for public release, distribution is unlimited.

13. SUPPLEMENTARY NOTES

14. ABSTRACT
Countercurrent flow control was applied as a novel flame stabilization technique on a premixed jet flame. In the experimental setup a converging nozzle burner was placed concentrically in a suction collar to generate suction driven countercurrent flow. Flame blow off velocity was measured at different suction velocity and equivalence ratio values. Tests show that by applying countercurrent flow around the periphery of a jet flame it can be stabilized up to jet exit velocity of 40 m/s. Particle Image Velocimetry (PIV) measurements and shadowgraph visualizations reveal that, application of suction changes the shear layer structure. An optical temperature measurement technique, refereed to as Laser Speckle Displacement (LSD) was developed for instantaneous temperature field measurements. It is shown that the technique is easy to implement and can be used in conjunction with PIV for simultaneous velocity and temperature measurements in reacting flows.

15. SUBJECT TERMS
Premixed jet flame, flame stabilization, countercurrent flow, speckle photography, particle image velocimetry

16. SECURITY CLASSIFICATION OF:			17. LIMITATION OF ABSTRACT	18. NUMBER OF PAGES	19a. NAME OF RESPONSIBLE PERSON
a. REPORT	b. ABSTRACT	c. THIS PAGE	SAR	45	Anjaneyulu Krothapalli
UU	UU	UU			19b. TELEPONE NUMBER *(Include area code)* 850-644-5885

FINAL REPORT

ACTIVE CONTROL OF HIGH SPEED JET FLAMES USING COUNTERFLOW

ONR CONTRACT NUMBER

N00014-98-1-0424

Submitted to

Propulsion Research Program
Office of Naval Research
800 North Quincy Street
Arlington, VA22217-5660

By

Department of Mechanical Engineering
FAMU-FSU College of Engineering
2525 Pottsdamer Street
Tallahassee, FL 32310

Principle investigators

Anjaneyulu Krothapalli, Ph.D.
Don Fuqua Eminent Scholar and Professor
and
Luiz M. Lourenco, Ph.D.
Professor

APRIL 2003

ABSTRACT

Countercurrent flow control was applied as a novel flame stabilization technique on a premixed jet flame. In the experimental setup a converging nozzle burner was placed concentrically in a suction collar to generate suction driven countercurrent flow. Flame blow off velocity was measured at different suction velocity and equivalence ratio values. Tests show that by applying countercurrent flow around the periphery of a jet flame it can be stabilized up to jet exit velocity of 40 m/s. Particle Image Velocimetry (PIV) measurements and shadowgraph visualizations reveal that, application of suction changes the shear layer structure. An optical temperature measurement technique, refereed to as Laser Speckle Displacement (LSD) was developed for instantaneous temperature field measurements. It is shown that the technique is easy to implement and can be used in conjunction with PIV for simultaneous velocity and temperature measurements in reacting flows.

Table of Contents

1. INTRODUCTION 1

1.1 Background 1

1.2 Objective 2

2. EXPERIMENTAL TECHNIQUES AND FACILITY 3

2.1 Low speed combustion facility 3

2.2 Measurement techniques 5

2.2.1 Particle Image Velocimetry (PIV) 5

2.2.2 Laser Speckle Displacement (LSD) technique 10

3. RESULTS 25

3.1 Flame stability 25

3.2 Countercurrent effect on the flow structure 31

3.3 Velocity field measurements by means of PIV 35

4. SUMMARY 40

References 41

1. INTRODUCTION

1.1 Background

Modern combustion and propulsion systems are required to operate at an increased energy density and a high turndown ratio (ratio of maximum to minimum flow rates). Requirement of wide operation range comes with the concern of maintaining stable flame conditions, at which the flame is "anchored" either at the burner rim or at some position downstream from the burner port, against *blow off*. B*low off* is an unstable flame phenomenon, which is defined as the transportation of the flame away from the burner port resulting in the extinction of the flame. *Blow off* occurs when the flow velocity in the shear layer exceeds the burning velocity of the flame at the burner exit causing the downstream propagation of the combustion wave. The flame stabilization techniques can be mainly grouped as stabilization by solid elements and stabilization by fluid streams (Williams 1985). Bluff body flame holders are the most common application of solid element stabilization. In bluff body stabilization, the flame is attached in the wake of solid elements, which is inserted in the main stream of the flow. The reduced flow velocity in the recirculation region formed in the wake of the bluff body helps in flame stabilization. Fluid stream stabilization is used either to enhance the performance of the bluff body flame holders or to maintain flame stabilization. Another important parameter in the stabilization of the turbulent flames is *mixing*. Especially in jet flames rather than the chemical reaction rate, the mixing process controls the rate of combustion. Appropriate modes of instability can be utilized to improve the mixing in the combustion process. Strykowski and Niccum (1991,1992) investigated the effect of suction driven countercurrent flow on the stability of shear layers for laminar cold jets, and they also presented the influence of velocity and density ratio on the mixing layer development. A study on the cold jets show that applying a countercurrent flow around the jet perimeter enhances the mixing between the jet and the surrounding fluid by establishing the self-excited global oscillations (Strykowski and Wilcoxon 1993). The control technique of countercurrent flow relies on the self-excitability of the jet without using complicated feedback control systems and actuators. The same technique was applied for supersonic shear layer control to increase the mixing (Strykowski and Krothapalli 1993). These studies suggest that the countercurrent control technique can be utilized to stabilize high-speed premixed jet flames. The main parameters that govern the maximum attainable blow

off velocity are strain rates at the nozzle exit and mixing of the fuel-air jet with the surrounding air. The countercurrent shear layer seems to produce the strain field in the nozzle exit region to achieve the conditions for flame anchoring and stabilization.

1.2 Objective

The main objective of this project is to introduce countercurrent flame stabilization as a novel control technique for flame anchoring at higher jet exit velocities. It is known that the maximum speed that can be achieved while keeping the flame anchored to the nozzle exit is determined by the maximum sustainable strain rate at the nozzle exit. Previous studies show that, by the introduction of a countercurrent flow, the strain field at the nozzle exit is effectively altered and a significant mixing enhancement is attained in cold and heated jets. By knowing that mechanism in the stabilization of the flame is hydrodynamic in nature, the objective of this study is to investigate the effect of countercurrent flow on flame *blow off* velocity and flow structure of a premixed jet flame by means of optical measurement techniques. Besides applying a novel control technique for the stabilization of a premixed jet flame, experimental investigation of the physical mechanism, which is responsible for the stabilization at high jet velocities, can form a basis for future flame stability studies.

In the investigation of flow field-combustion interaction, non-intrusive temperature measurements, or simultaneous temperature and velocity measurements are necessary for better understanding of the problem. In this study a PIV system that was developed in Fluid Mechanics Research Laboratory was used for velocity field measurements. In addition, an affordable and simple optical technique for temperature measurement is developed and successfully implemented in this study.

2. EXPERIMENTAL TECHNIQUES AND FACILITY

2.1 Low speed combustion facility

A new jet flame facility was built in the Fluid Mechanics Research Laboratory for the studies discussed here. This facility consists of a low speed nozzle burner with a circular cross-section, which is placed concentrically into the suction collar as shown in figure 2.1. The burner is manufactured from stainless steel by using a fourth order polynomial contour with the zero slope and zero curvature conditions at the nozzle inlet and exit. The nozzle contraction ratio is 26 with a nozzle exit diameter, D= 10.16 mm. The suction collar surrounding the nozzle has the dimensions of W/D = 0.18 and L/D =1.0, where W is the gap between the inner wall of the suction collar and nozzle, and L is the height of the suction collar. The geometric parameters W and L were varied to examine their effect on blow off velocity. Typical results of the blow of velocity for different configurations are shown in figure 2.2. Based on these observations, the geometric parameters mentioned above were chosen for the detailed study.

The primary jet is obtained by feeding propane-air mixture through the nozzle. Counterflow is maintained by applying suction around the perimeter of the nozzle. A manifold consisting of 8 equally positioned ports is used to draw the air, by means of a suction pump, through the gap between the suction collar and the nozzle uniformly. Each suction port is equipped with a solenoid valve for the unsteady suction applications. Air and fuel flow rates are measured separately prior to mixing. The primary jet exit velocity U_1 is calculated from fuel and air flow rate measurements. The measured countercurrent mass flow rate is used to calculate the average suction velocity U_2. Before entering the nozzle, fuel and air are mixed in a mixing chamber to assure the homogeneous air-fuel mixture.

One of the most essential requisite in implementation of PIV is the flow seeding. In order to obtain acceptable accuracy, the seeding particles must be approximately equivalent in size and they must be evenly distributed in the flow field. A fluidized bed seeder is designed and built specifically for this purpose. A rotating hollow tube with paddles continuously stirs solid particles in powder form. High-pressure air is send through the hollow tube into the powder bath to create the solid particle aerosol. Solid particle seeding is particularly necessary for high temperature or combustion flows. The commonly used solid particles are abrasives like aluminum oxide, magnesium oxide or titanium dioxide, which are in the order of 0.1 micron in size and resistant to high flame temperatures.

In the present experimental set-up, two fluidized bed seeders are used to seed both the fuel-air mixture jet and the surrounding air. Aluminum oxide powder with the particle diameter of 0.3 μm is used in the seeders. Before mixing the fuel and the air, air is metered by means of a mass flow meter and then it is passed through the seeder. To maintain the good seeding in the ambient air, a confinement chamber is placed around the flame as seen in figure 2.4, and seeded air is supplied to its settling chamber at a very low flow rate. The co-flow jet velocity is typically maintained at one meter per second. The confinement chamber is made of eight Pyrex windows.

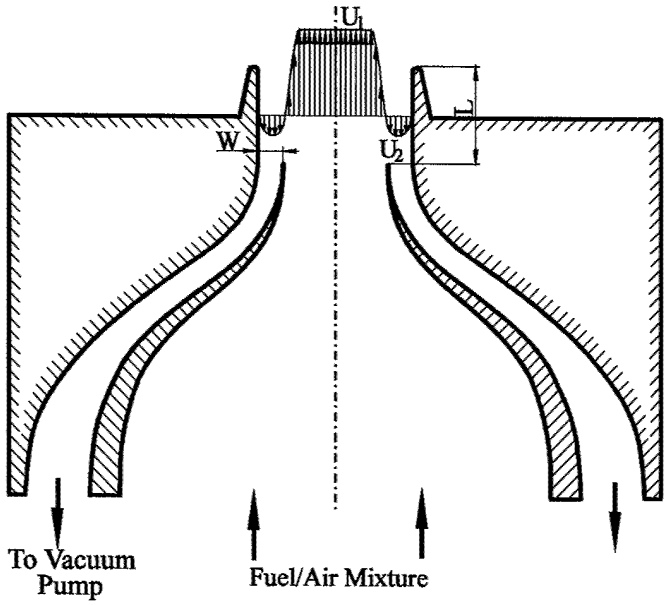

Figure 2.1 Nozzle suction collar configuration

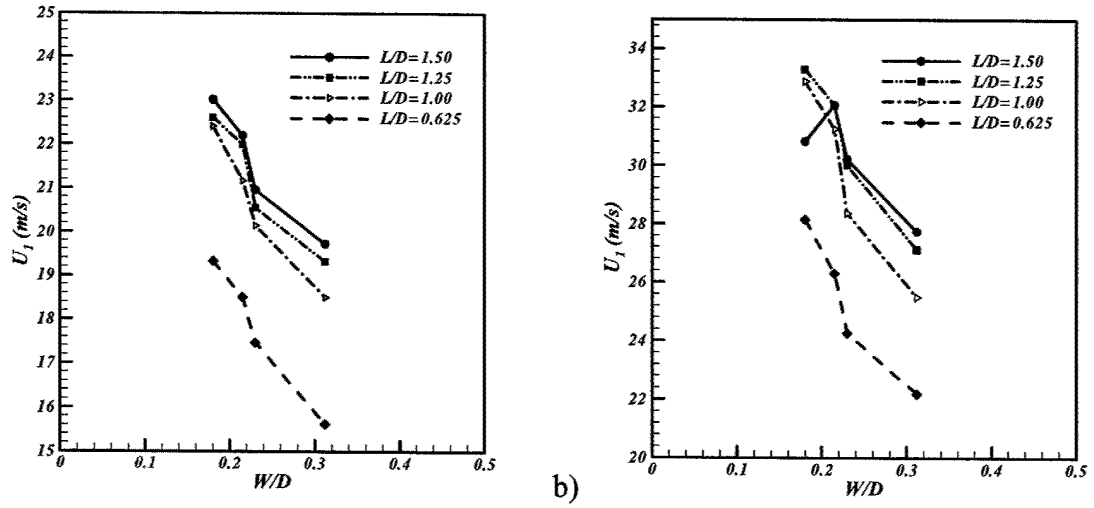

Figure 2.2. Blow off velocity change with suction collar dimensions at constant fuel flow rates a) $Q_{fuel}=13.29x10^{-5}$ m^3/s, b) $Q_{fuel}=33.22x10^{-5}$ m^3/s

2.2 Measurement techniques

2.2.1 Stereoscopic Particle Image Velocimetry

Stereo viewing of the object plane is the key to obtain the three-dimensional vector field from the projected image views of the measurement plane. Each view has an angle with respect to the object plane. Unlike the case of a two-dimensional imaging with a lens, which is oriented to the object plane, off-axis imaging involves some complex relationships between the position of the object points and their corresponding positions in the image plane. The focusing on the object plane with the off-axis positioning of the lens can be achieved by using the Scheimpflug condition [Alkislar et al. 2000]. Figure 2.3 illustrates the sharpness of the focusing depending on the lens orientation. Figure 2.3(a) shows the imaging lens and object plane orientation for the conventional imaging, which gives uniform magnification and sharp focus in the whole field. However, as in picture (b), when the imaging lens is placed in an off axis position at which it makes an angle with the object plane while it is parallel to the imaging plane, the image is well focused at the center, but at the sides it is unacceptably out of focus. To overcome defocusing effect of the off axis positioning the Scheimpflug condition, shown in picture (c), must be applied. The Scheimpflug condition ensures perfect focusing on an entire field when the object plane, the imaging lens plane and the image plane intersect at a point. On the other hand, contrary to conventional imaging, the magnification is not uniform in the image plane, which requires the magnification calibration on the object plane.

The 3-D PIV setup uses two Kodak ES 1.0 cameras. The CCD cameras have a resolution of 1008(H)×1018(V) pixels with the size of 9×9 μm, and a maximum frame rate of 30 Hz. The cameras are equipped with specially designed lenses with 58.37*mm* focal length that is specifically designed for the wavelength of the laser light, and they are seated on precise linear and angular positioning stages. A microcomputer, with two PentiumPro CPU's, controls the dual camera arrangement, and is capable of acquiring up to 128 image pairs per camera, at the maximum frame rate. To illuminate the flow-field, New Wave Gemini PIV, Nd-Yag laser with dual cavity, 15 Hz frequency and 500mJ power is used synchronized with the cameras. The time Δt between the two laser pulses is changed in the range of 35–100 μsec.

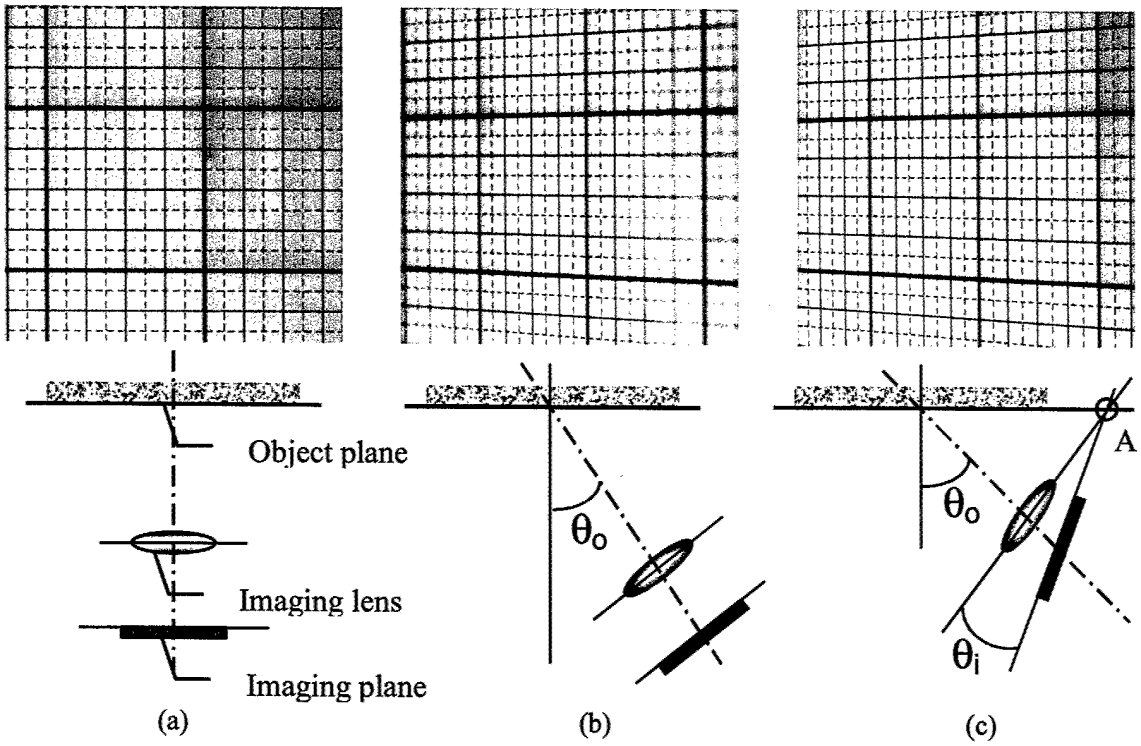

Figure 2.3. Precise focus on the object plane applying Scheimpflug condition

For the imaging of the streamwise flow field, two cameras are mounted on the same horizontal rail. Each camera is positioned at a certain angle, θ_o, from the normal of measurement plane to obtain a stereo view of the plane as shown in figure 2.5. To attain sharp focus on the entire measurement plane, each camera is rotated with respect to the lens plane at an angle of θ_i satisfying the Scheimpflug condition for off-axis imaging. In stereo imaging of a flow field there are two view modes; the same side imaging which is convenient for cross plane measurements and the opposite side imaging suitable for streamwise measurements (Alkislar 2001). In the experiments, despite the streamwise measurements, because of the space limitations same side imaging arrangement is used. In this arrangement while one of the cameras receives the light with forward scattering, the other one receives with backward scattering by causing different light intensities on the images. To obtain the images at the same quality, an arrangement of natural density light filters is placed before the forward receiving camera lens. Another important component of the camera lens arrangement for PIV measurements in combustion is the band pass filter for the laser wavelength of 532 nm, which is necessary to filter the flame radiation. Both cameras are pre-calibrated collectively before the experiment. After processing the images acquired by each camera, the data from each view are combined to give the three-component

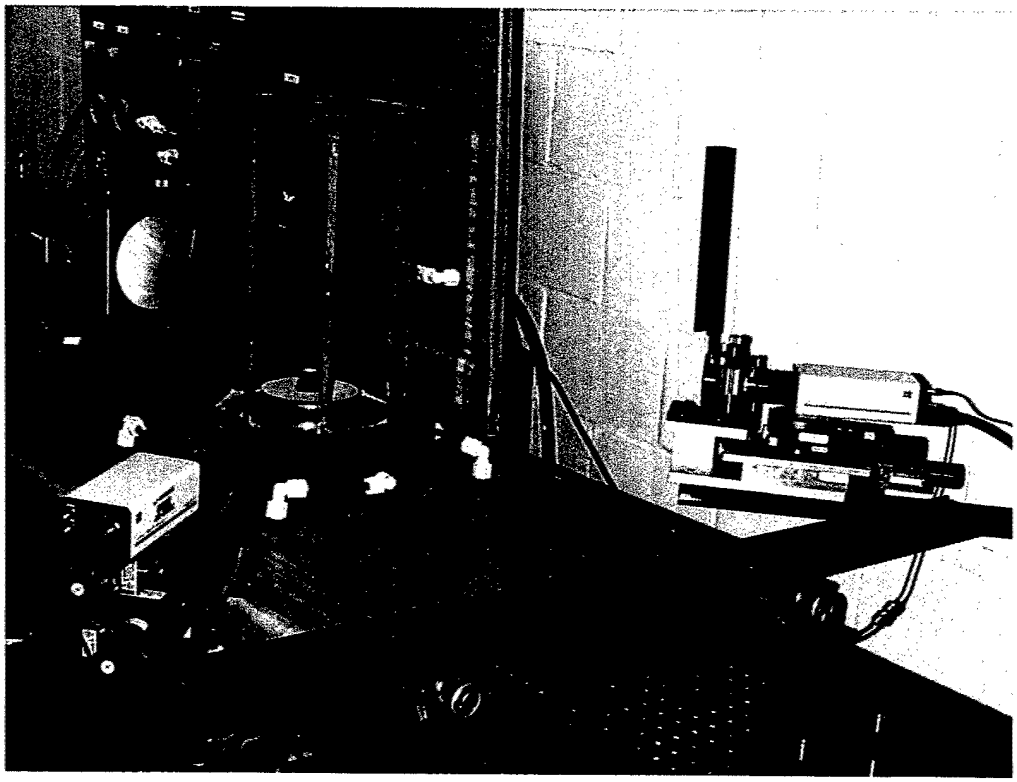

Figure 2.4. Stereoscopic positioning of the cameras for 3-D PIV.

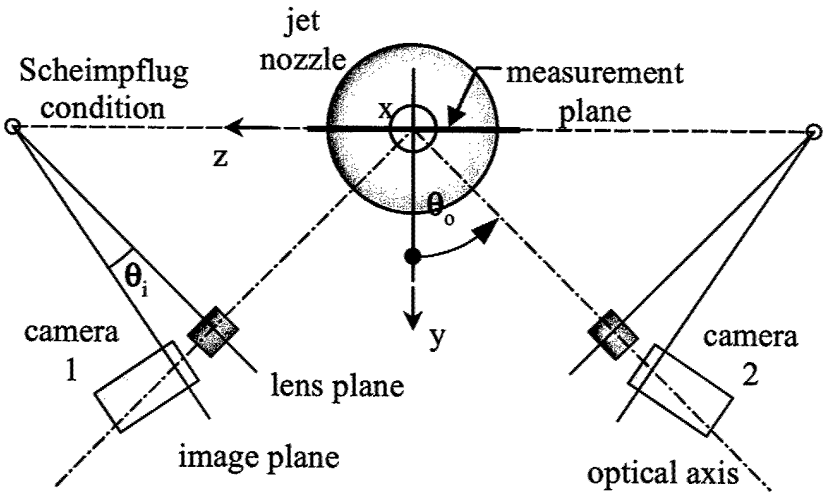

Figure 2.5. Off-axis positioning of cameras for 3-D PIV.

velocity field at the measurement plane. The equations that govern both the transformation of the image plane to the object plane and the combination of the data from both views to yield a three-dimensional velocity field is given by Alkislar (2001).

A sample stereoscopic PIV image and the corresponding vector fields of in plane velocity components are shown in figure 2.6. These 2D vector fields are used in the reconstruction of the out of plane velocity component as shown in figure 2.7.

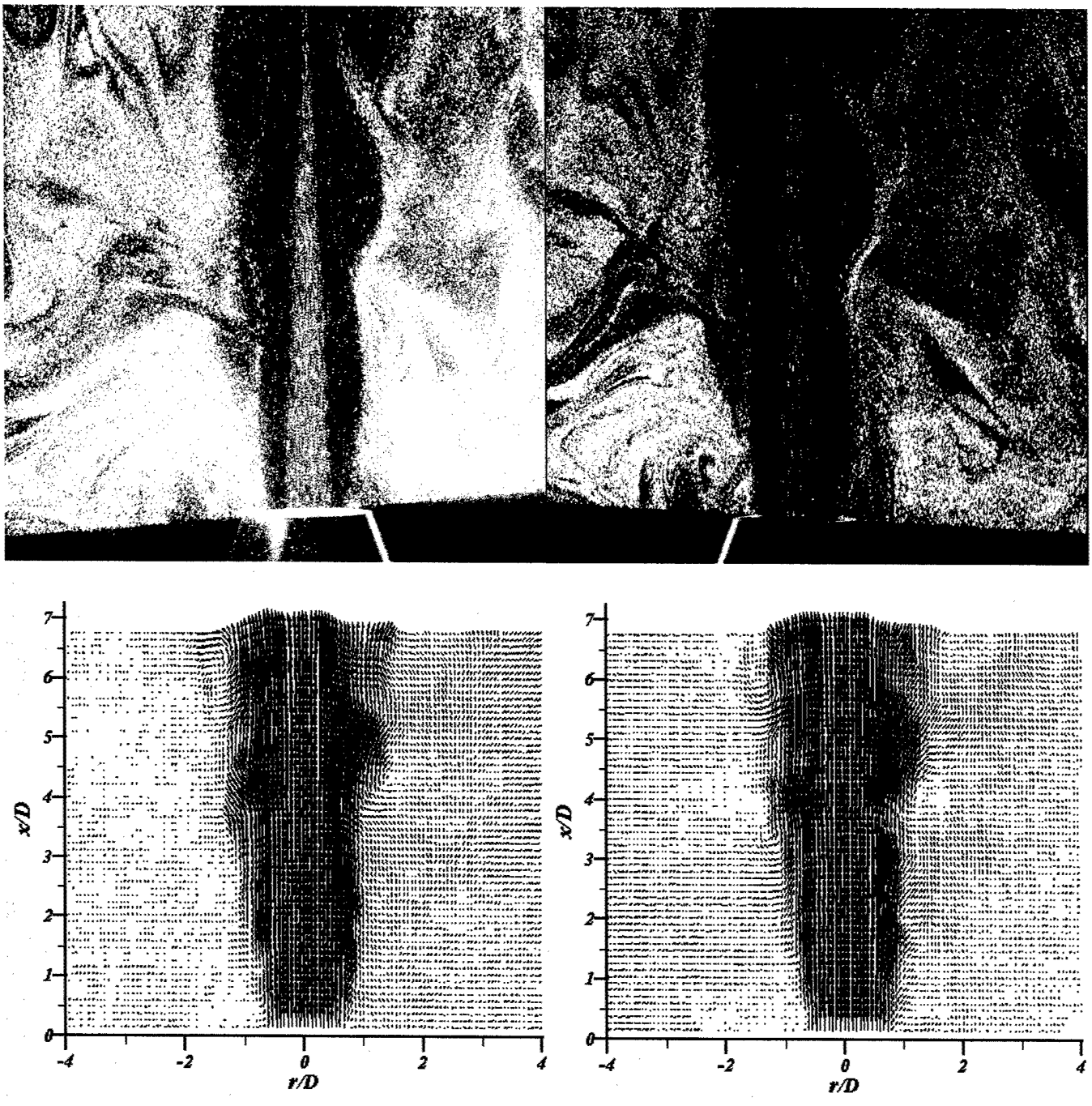

Figure 2.6. A sample stereoscopic PIV image and vector fields corresponding to each camera view.

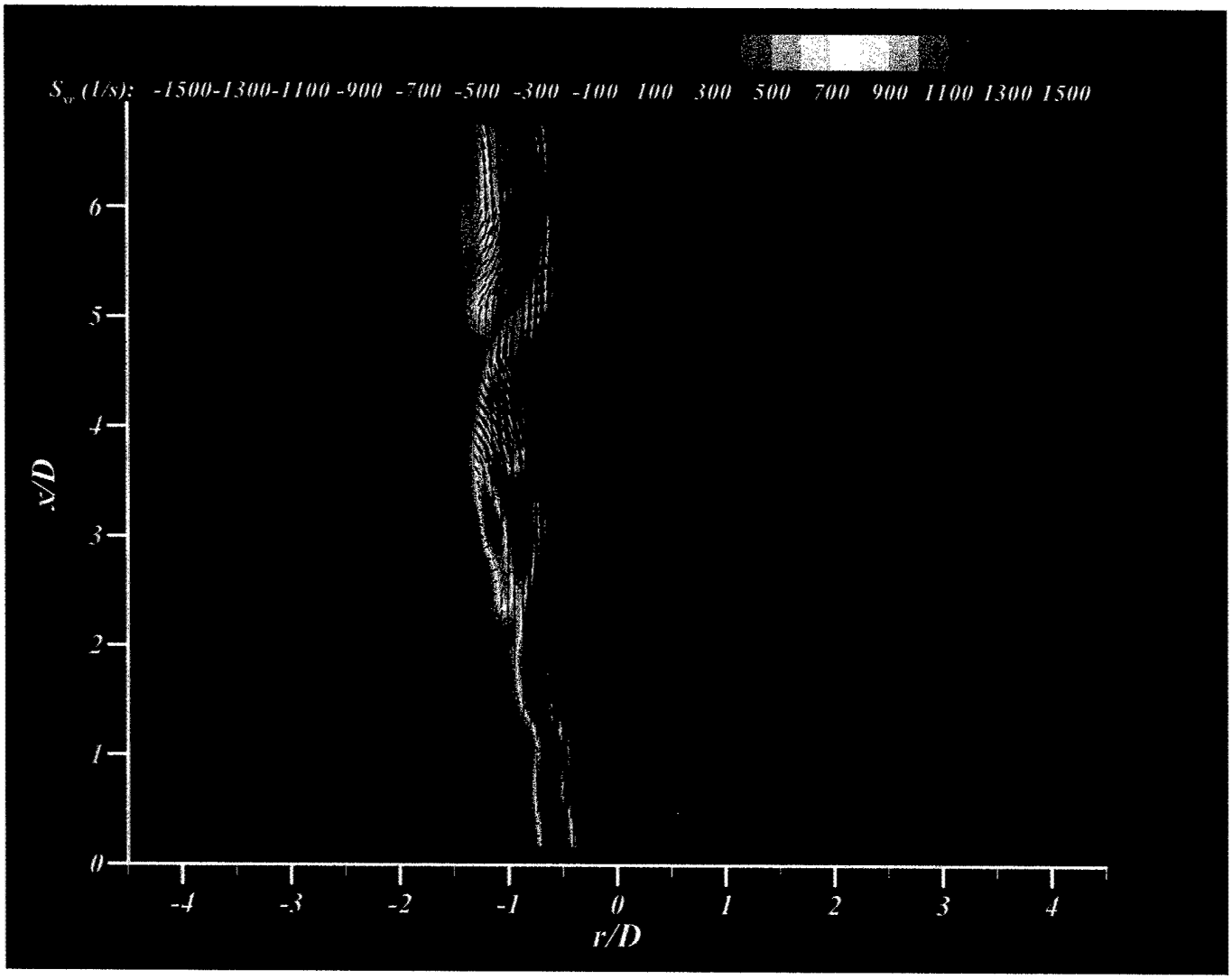

Figure 2.7. Projection of 3D vector field superposed with the strain rate contours.

2.2.2 Laser Speckle Displacement (LSD) technique

The investigation of flow fields with significant temperature or density variations, such as compressible flows and flames, requires the measurement of these parameters. Non-intrusive measurement of temperature and density is made possible by the development of optical measurement techniques. Dynamic light scattering, laser induced fluorescence and infrared thermography are several of optical temperature measurement techniques. However, the complexity and high cost of optical setups (Gebhard et al. 1994) put these techniques beyond the limits of practicability. With recent advances in computer and image recording technology, speckle photography stands out as a promising non-intrusive technique. Speckle photography uses the beam deflection theory (Born and Wolf 1980) for the measurement of temperature and density from refractive index variations in a flow field. When a laser beam illuminates a diffuse object, the surface of the object appears to have a fine granular structure, which is known as speckle, and a speckle pattern can be observed in a plane located at a distance L from the diffuse object. Each diffuse object has its own signature speckle pattern regardless of the incident angle of the light beam. When the incident beam is deflected by an angle of θ, it produces the same speckle pattern on the observation plane, but only translated by a distance of θL (Francon 1979). The deflection of the incident beam can be determined by measuring the translation in the speckle location. Since the deflection of beam in a phase medium is a result of refractive index variations, the relationship between these two is expressed by beam deflection theory. Therefore, the refractive index variations can be calculated from measured beam deflection angles (Fomin 1998).

In the early stages of speckle photography an attempt was made to determine the deflection of a light ray with an optical arrangement, which was simpler than the interferometry set-up. Debrus et al.(1972) applied the basic principle of speckle photography by using a white light to establish the refractive index changes around a heated metallic road. Because of the incoherent light source only the visualization of the refractive index field was obtained. However, using laser light in the formation of speckle pattern made it possible to determine deflection of light ray quantitatively in the existence of a phase object (Kopf 1972). During the last three decades speckle photography was applied in various fluid mechanics and combustion problems for both rectangular and cylindrical flow fields and these studies demonstrate that, the

technique can generate qualitative results (Farrell and Hofeldt 1984, Erbeck and Merzkirch 1988, Keller and Merzkirch 1990, Shakher et al. 1994, Fomin et al. 1999, Alkislar 2001).

In the application of speckle photography, mathematical manipulation of the data and the assumptions made in the derivation of ray tracing equations has great importance. In the case of weak refraction, equations take a simplified form with the paraxial approximation and with the assumption of small deflection angles compared to characteristic length of the flow field (Fomin 1998). Since calculation of local temperature values in a flow field requires the integration of beam deflection angles along the beam path, the application of the technique for flow fields with a cross section other than rectangle leads to complex data manipulations. In a flow field with a circular cross section calculation of local refractive index values requires the evaluation of inverse Abel integral. Singular behavior of the integrand at $r = 0$ and requirement of spatial differentiation of data makes the practical application of inverse Abel integral difficult (Rubinstein and Greenberg 1993). Since in speckle photography the measured deflection angles are physically associated with the gradient of the refractive index it is possible to avoid spatial differentiation of the data. The trade off in the application is, for temperature measurements the vertical beam deviation has to be assumed negligible. Farrell and Hofeldt (1984) used speckle photography to measure temperature distribution in an axisymmetric propane flame with the application of inverse Abel transform. However, their study was limited by the spatial resolution of deflection data. As a result of limited experimental data, they evaluated inverse Abel integral by applying the method of Cremers and Birkebak (1966), which requires piecewise least-square curve fitting and they only considered the beam deflection in horizontal direction.

In the early studies of speckle photography the speckle images were recorded on a photographic medium. Although the resolution of photographic recording is high, the Young's fringe analysis of images is time consuming and due to long processing time is not practical. With the recent advances in digital image recording and processing, digital speckle photography was introduced. In the present study a novel application of digital speckle photography, called laser speckle displacement (LSD) technique, is used for the instantaneous and the averaged temperature field measurements in an axisymmetric jet flame. In LSD, beam deflection angles are measured in terms of speckle displacements and opposed to previous speckle photography measurements both horizontal and vertical displacements are used in the calculation of temperature field. Alkislar (2001) introduced the idea of incorporating both displacement

components in the solution of Poisson equation and applied the technique for density measurements in a rectangular supersonic jet. The use of digital image acquisition and accurate cross correlation processing scheme developed by Lourenco and Krothapalli (2000) enables us to obtain displacement field on a very fine mesh. Therefore, spatial differentiation of experimental data in the evaluation of inverse Abel transform can be easily applied to calculate the refractive index gradient in the whole measurement field. The refractive index variations in horizontal and vertical directions are used in the numerical solution of Poisson equation to obtain the field distribution of refractive index, which is related to temperature by Gladstone-Dale or Lorentz-Lorenz relationship.

In this report the approach taken to implement LSD technique is explained with the results of an axisymmetric jet flame. This technique in conjunction with PIV is used to measure simultaneous temperature and velocity fields.

Theoretical background

The deflection of light in the presence of a medium is proportional to the change of refractive index. The differential equation, which relates the beam path directly to the refractive index, can be written as in equation1 (Born and Wolf 1980). In the equation, position coordinates of a typical point on the beam path is denoted by a vector $\mathbf{r} = u\,\mathbf{i}+v\,\mathbf{j}+w\,\mathbf{k}$, s is the length of the path measured from a fixed point on the path, and n is refractive index.

$$\frac{d}{ds}\left(n\frac{d\mathbf{r}}{ds}\right)=\nabla n \tag{1}$$

Alternatively in equation 2, the rate of change of beam direction, ds, is expressed in terms of refractive index change along the path.

$$\frac{d\mathbf{s}}{ds}=\nabla\overline{n} \tag{2}$$

where

$$\overline{n}=\ln(n) \tag{3}$$

The coordinate system and the notation of variables used in the derivations are given in figure 2.8. From equation 2, light beam deflection through the flow field, θ, can be expressed as

an integral in rectangular coordinates, where $\mathbf{S_1}$ and $\mathbf{S_2}$ are the inlet and the exit points of the beam respectively.

$$\theta(x,z) = \int_{S_1}^{S_2} \nabla \bar{n}(x,y,z)ds \tag{4}$$

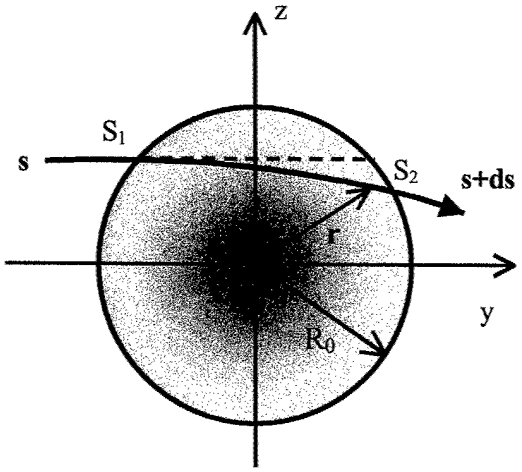

Figure 2.8. Laser beam deviation in circular flow fields.

With the assumptions of uniform and homogeneous ambient conditions, paraxial beam path, and small deflections with respect to flow dimensions, horizontal and vertical components of a deflection angle can be written as the integral of refractive index changes

$$\theta_x(x,z) = \int_{-\infty}^{+\infty} \frac{\partial \bar{n}}{\partial x} dy \tag{5}$$

$$\theta_z(x,z) = \int_{-\infty}^{+\infty} \frac{\partial \bar{n}}{\partial z} dy \tag{6}$$

For a circular axisymmetric flow field, shown in figure 2.8, equations 5 and 6 are rewritten in cylindrical coordinates by using $r^2 = y^2 + z^2$.

$$\theta_x(x,r) = 2\int_{|z|}^{+\infty} \frac{\partial \overline{n}}{\partial x} \frac{r}{\sqrt{r^2 - z^2}} dr \tag{7}$$

$$\theta_z(x,r) = 2z\int_{|z|}^{+\infty} \frac{1}{r}\frac{\partial \overline{n}}{\partial r} \frac{r}{\sqrt{r^2 - z^2}} dr \tag{8}$$

When equations 7 and 8 are rearranged by using r as the variable, they can be rewritten in the form of Abel integral (Fomin1998). By applying inverse Abel transform the refractive index gradients in axial and radial directions are expressed in terms of measured axial and transverse beam deflection angles. In the application of speckle photography, deflection angles are measured experimentally in terms of displacement components to calculate the refractive index values in the flow field. To apply equations 7 and 8 to the experimental data upper limit of integration is changed as R_0, the location at which the refractive index gradient is zero and it is the radial distance measured from the jet centerline (figure 2.8). Finally, equations that are used to calculate the refractive index gradients take the following form

$$\frac{\partial \overline{n}}{\partial x} = -\frac{1}{\pi}\int_{r}^{R_0} \frac{\partial \theta_x}{\partial z} \frac{1}{\sqrt{z^2 - r^2}} dz \tag{9}$$

$$\frac{\partial \overline{n}}{\partial r} = -\frac{1}{\pi}\int_{r}^{R_0} \frac{\partial}{\partial z}\left(\frac{\theta_z}{z}\right) \frac{1}{\sqrt{z^2 - r^2}} dz \tag{10}$$

As seen in equations 9 and 10 integrals have a singular point at $z = r$. Singularity is removed by dividing the integration into two parts and the first integral is evaluated over a very small interval of $[r,r+\delta]$ by using the approximation $f(z) = f(r) + (z-r)f'(r)$ for any function $f(z)$ (Fomin 1998).

In the proposed method, refractive index variations are calculated by solving the Poisson equation over the measurement field with the given boundary conditions (equations 11 and 12).

$$\nabla^2 \bar{n} = \frac{\partial^2 \bar{n}}{\partial \eta^2} + \frac{\partial^2 \bar{n}}{\partial \zeta^2} = \mathrm{F}(\eta, \zeta) \tag{11}$$

Boundary conditions

$$\begin{aligned}
&\eta = 0 && \bar{n}(0,\zeta) = \bar{n}_0 \\
&\eta = 2R_0 && \bar{n}(2R_0,\zeta) = \bar{n}_0 \\
&\zeta = 0 && \frac{\partial \bar{n}}{\partial \zeta} = \frac{\partial \bar{n}}{\partial \zeta}\bigg|_{\eta,0} \\
&\zeta = \zeta_1 && \frac{\partial \bar{n}}{\partial \zeta} = \frac{\partial \bar{n}}{\partial \zeta}\bigg|_{\eta,\zeta_1}
\end{aligned} \tag{12}$$

When both sides of the Poisson equation are discritized as in equations 13 and 14, the source function $\mathrm{F}(\eta,\zeta)$ is described in terms of refractive index gradients at each point.

$$\nabla^2 \bar{n} = \frac{\bar{n}_{i+1,j} - 2\bar{n}_{i,j} + \bar{n}_{i-1,j}}{\Delta\eta^2} + \frac{\bar{n}_{i,j+1} - 2\bar{n}_{i,j} + \bar{n}_{i,j-1}}{\Delta\zeta^2} \tag{13}$$

$$F_{ij} = \frac{\left(\frac{\partial \bar{n}}{\partial \eta}\right)_{i+1,j} - \left(\frac{\partial \bar{n}}{\partial \eta}\right)_{i-1,j}}{2\Delta\eta} + \frac{\left(\frac{\partial \bar{n}}{\partial \zeta}\right)_{i,j+1} - \left(\frac{\partial \bar{n}}{\partial \zeta}\right)_{i,j-1}}{2\Delta\zeta} \tag{14}$$

As seen in equation 14, refractive index gradients in horizontal and vertical directions are needed to obtain $\mathbf{F}(\eta,\zeta)$. At each grid point these values are calculated by using equations 9 and 10, which are derived from the beam deflection theory. Calculated source terms are substituted in the discritized Poisson equation for the iterative numerical solution of $\overline{n}(\eta,\zeta)-\overline{n}_0$, which is the difference between the local refractive index and the reference refractive index calculated at $r=R_0$. As a numerical method, line successive over relaxation (LSOR) is applied to whole flow field by shifting the origin of the rectangular coordinate system to the left corner of the measurement field, where, $\eta = z + R_0$ and $\zeta = x$.

The relationship between the refractive index gradient and the temperature for a pure gas is given by the Lorenz-Lorentz equation or alternatively by the Gladstone-Dale equation. As shown in equation 15, the Lorenz-Lorentz equation defines the molar refractivity, R_L, of a pure gas in terms of the refractive index and the molar density, ρ, of the gas at the temperature and pressure at which n is measured.

$$R_L = \frac{n^2-1}{n^2+2}\cdot\frac{1}{\rho} \tag{15}$$

The local molar refractivity of a gas can be computed from local major species concentrations. For a gas containing N significantly contributing species average molar refractivity can be calculated from

$$< R_L >= \sum_{i=1}^{N} R_{L_i} X_i \tag{16}$$

where X_i is the molar fraction of species i. Molar refractivity of combustion gases is tabulated by Gardiner et al. (1981) for different laser wavelengths. Solving equation 15 for the refractive index of a gas mixture results

$$n = \left(\frac{1+2\rho < R_L >}{1-\rho < R_L >}\right)^{1/2} \tag{17}$$

Since the molar density of the gas is calculated from ideal gas equation, local refractive index can be expressed as

$$n = \left(\frac{\overline{R}T/P + 2 < R_L >}{\overline{R}T/P - < R_L >} \right)^{1/2} \tag{18}$$

where T and P are the local temperature and pressure respectively, and $\overline{R}$ is the universal gas constant.

In the experiments temperature at the boundary of the flow field is measured by means of a thermocouple to calculate the reference refractive index, $\overline{n}_0$, at the boundaries $\eta = 0$ and $\eta = 2R_0$. It is assumed that at the boundaries there is no significant amount of combustion gases and reference refractive index is calculated for air at the measured temperature and atmospheric pressure.

Image recording and processing

In the experiments Gemini Nd-YAG laser was used as a coherent light source to benefit from its short duration of illumination for instantaneous temperature measurements. For the formation of speckle pattern the optical arrangement proposed by Wernekinck and Merzkirch (1987) was used with 1:1 magnification of the flow field on the ground glass. A schematic of the optical arrangement is shown in figure 2.9. First the laser beam was expanded with the help of a microscopic objective of power 20 and numerical aperture (NA) 0.40 along with a 15 μm spatial filter and then beam was collimated by a plano-convex lens, with the focal length (f_1) of 250 mm before it passed through the flame. Another plano-convex lens, focal length (f_2) of 450 mm, was used for imaging purpose to focus the light rays on the ground glass, which was placed $2f_2$ away from the imaging lens.

In acquisition of images, a particle image velocimetry (PIV) system, developed in FMRL, was used with a SharpVISION 1400DE camera. The CCD camera has a resolution of 1360(H) x 1024(V) pixels with a pixel size of 6.7μm X 6.7μm, and a maximum frame rate of 5 Hz. A Pentium IV microcomputer, with dual CPU, controls the camera and is capable of acquiring up to 256 image pairs at the maximum camera rate. In the experiments CCD camera was equipped with a 532-nm band pass filter and a 28-90 mm focusing lens with the zoom ratio of 3:1. To

capture large enough displacements for accurate processing, the camera was focused on a plane L distance away from the ground glass. The distorted grid calibration utility of the PIV system enables us to consider optical distortions in the images. To calibrate the magnification on the focusing plane and the optical distortions a rectangular plate with equally spaced holes was placed at the centerline of the circular burner. The image of calibration object was recorded by illuminating the calibration object with collimated laser beam. The free mesh used in calibration of distorted images is fitted on the bright spots of the calibration image. In figure 2.10 the calibration grid is shown with the half plane fitted mesh. Calibration of the images determines the original positions of the speckles and the magnification factor of the camera lens.

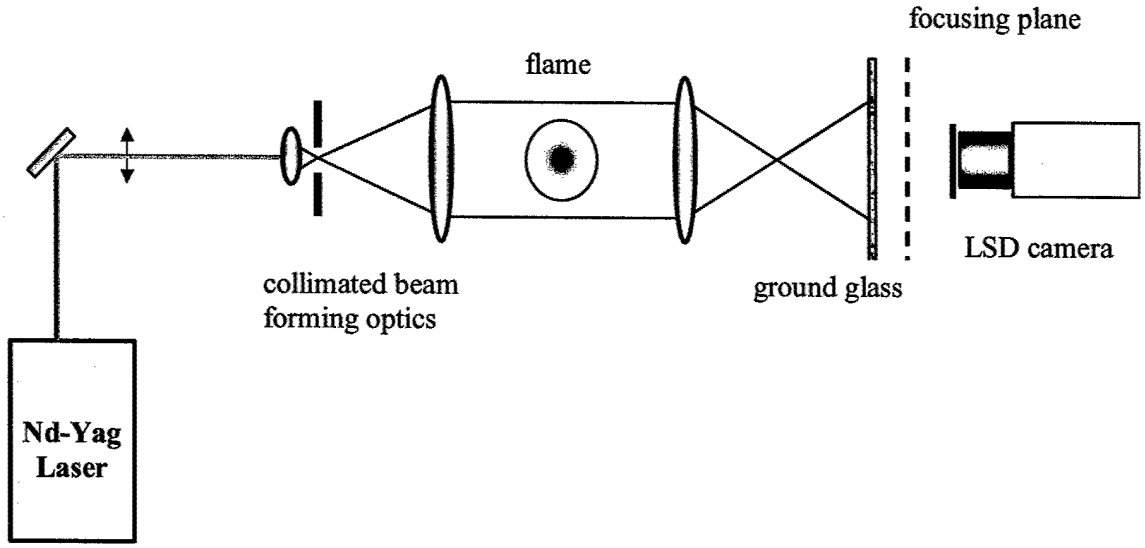

Figure 2.9. Schematic of the optical arrangement.

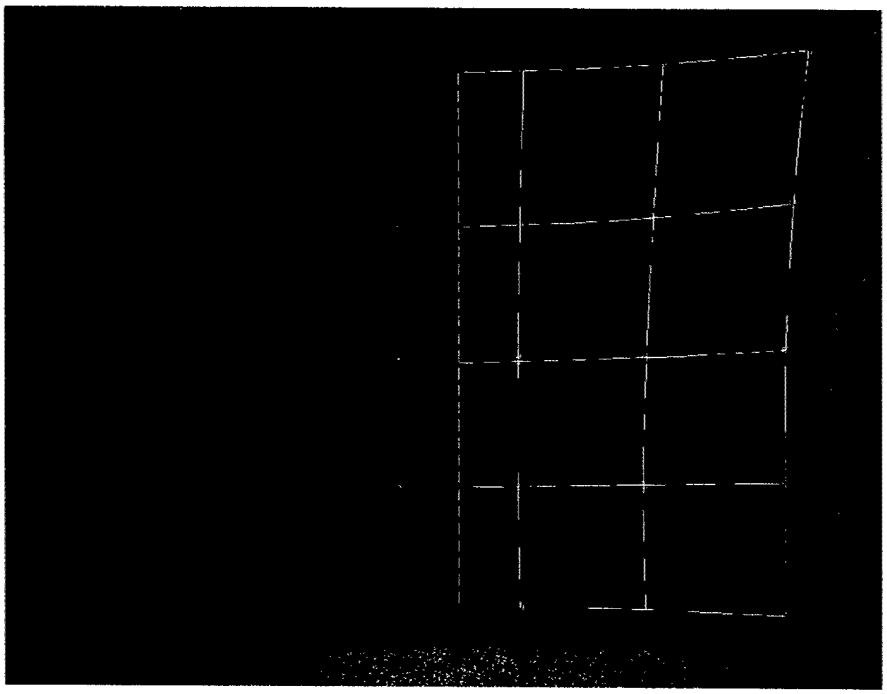

Figure 2.10. LSD calibration image and distorted calibration mesh (shown as half plane)

LSD technique is based on the measurement of refractive index changes with reference to the quiescent and isothermal ambient condition. In the acquisition of images first a reference speckle pattern is recorded without the flame. The speckle images corresponding to jet flame are acquired as a sequence of 1000 images. For the processing of data each speckle image is paired with the reference speckle image by marking reference image as the first and flame image as the second one. A sample image pair is shown in figure 2.11. Cross-correlation image processing between the reference speckle pattern and the flame speckle pattern determines the distance between the first and the second image of a speckle as a displacement vector in the whole flow field without directional ambiguity. The displacement vector field in figure 2.12 corresponds to sample LSD image pair and each vector represents the local rate of change of beam direction. The image processing utility applies a novel mesh-free, second order accurate, processing algorithm developed by Lourenco and Krothapalli (2000). This algorithm was designed to improve the accuracy and spatial resolution of conventional cross-correlation schemes. The high resolution and accuracy also provide second order accurate derivatives of displacements, which are the most important parameters used in the computation of the temperature fields.

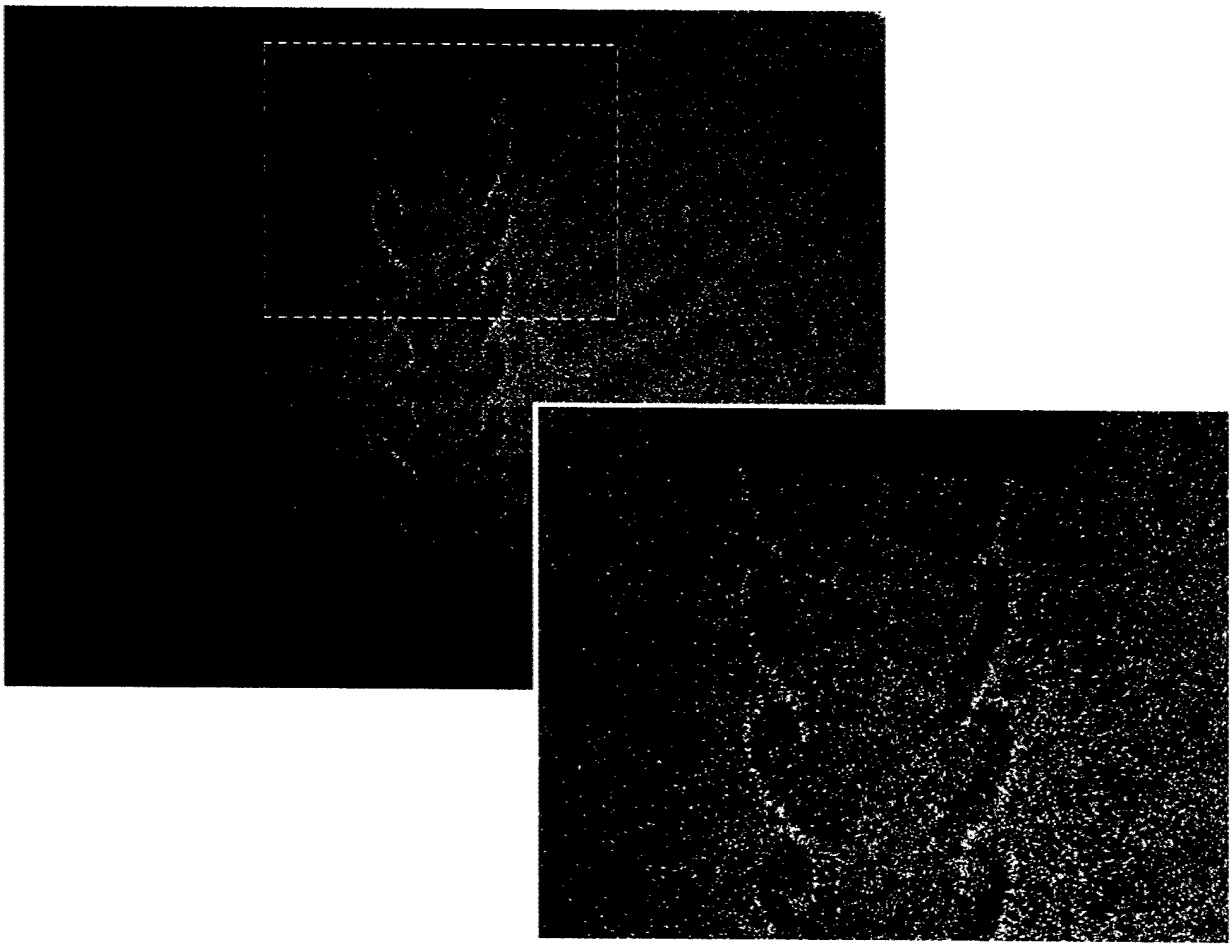

Figure 2.11. A sample whole field LSD image.

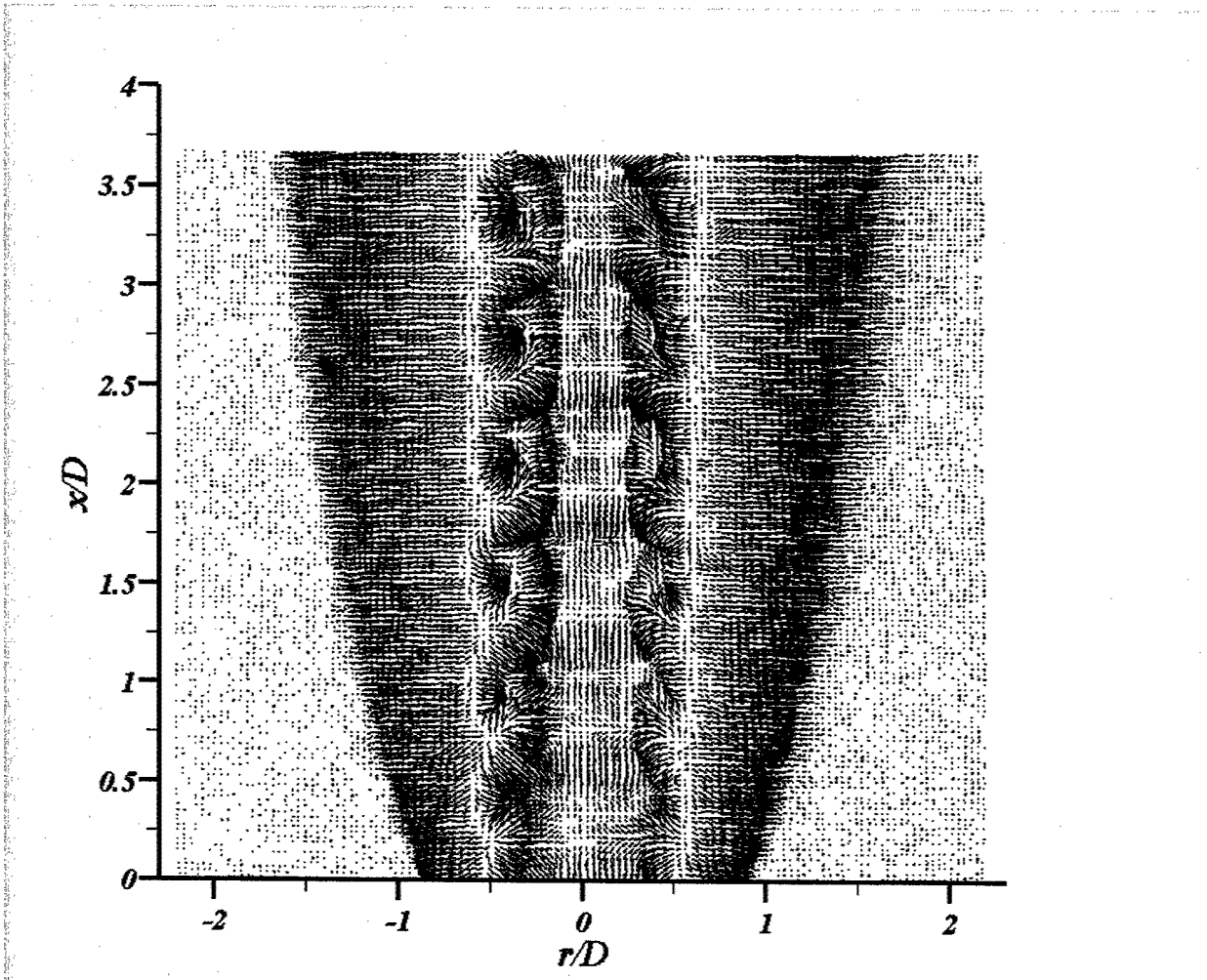

Figure 2.12. Displacement vector field corresponding to sample image pair

Test case: simultaneous LSD and PIV measurements

Purpose of simultaneous measurements is to test whether LSD method can capture the characteristic structures of the flame by comparing temperature field results with the corresponding velocity field. Therefore, an axisymmetric, laminar, naturally stable, and rich propane-air jet flame was chosen as a test case. First, the shadowgraph visualization of the flame was recorded to show the distinctive structures in the flow field as seen in figure 2.13.

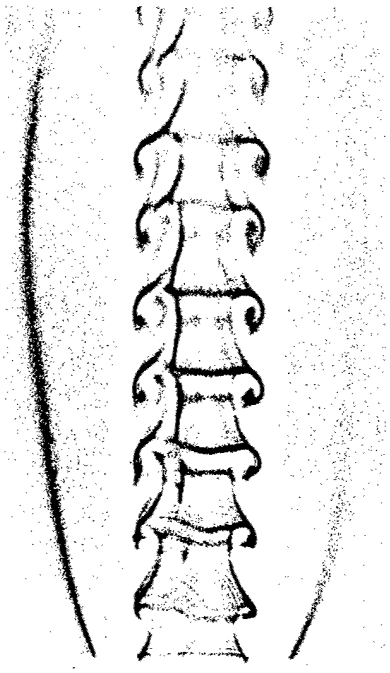

Figure 2.13. Shadowgraph visualization of axisymmetric, laminar jet flame

In this case, the jet velocity at the exit of the nozzle, U_1, was 5.3 m/s and the equivalence ratio was 3.0. In PIV measurements only the jet flame was seeded by aluminum oxide (Al_3O_2) particles, which was sufficient for observing vortical structures in the preheat region. In measurements an optical arrangement was set for two reasons: to create a speckle pattern for LSD technique, and to form a laser sheet for PIV measurement. As shown in figure 2.14, the laser beam is divided into two by means of a beam splitter and the power of the beam in the LSD side is decreased with the help of a polarizer. While the optical arrangement for LSD is the same as explained before, the second laser beam coming out of the beam splitter is projected towards the center of nozzle to form a laser sheet for PIV measurements. As sheet forming optics a convex lens is used together with a cylindrical lens.

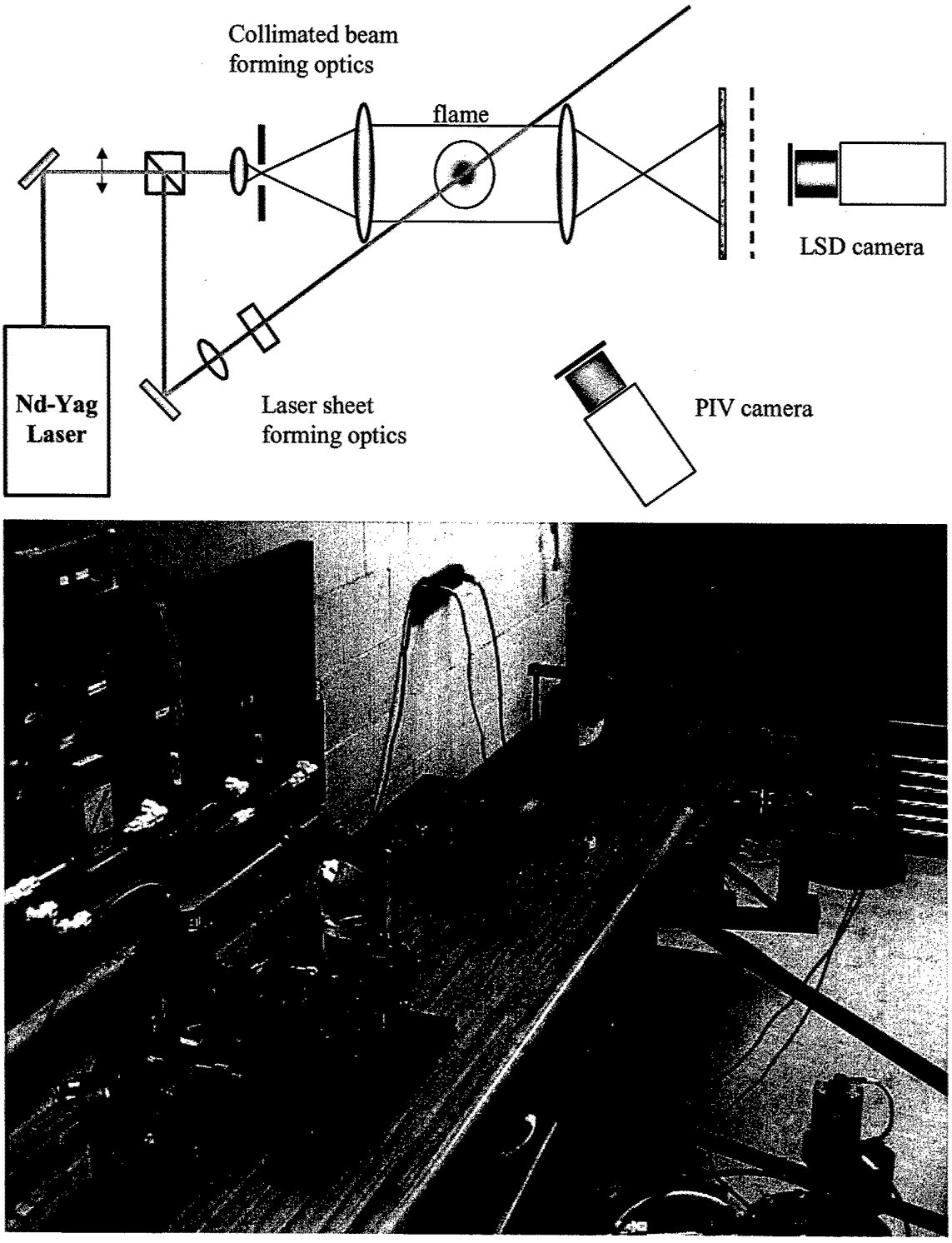

Figure 2.14. Optics and camera arrangement for simultaneous LSD and PIV measurements.

In acquisition of images, a 3-D PIV system is used with two sharpVISION 1400DE cameras. A Pentium IV microcomputer, with dual CPU, controls the dual camera arrangement, and is capable of acquiring up to 256 image pairs, at the maximum camera rate. Each CCD camera is equipped with a 532-nm band pass filter. LSD camera is used with a 67 mm zoom lens while PIV camera is equipped with a 55 mm lens and it is positioned perpendicular to the laser sheet. Processing of images are done as explained in previous sections. An example of simultaneous measurements is shown in figure 2.15 as half plane velocity vectors and half plane temperature field. The vortices of the flow are emphasized by vorticity contour plots on the velocity side and by velocity vectors on the temperature. As seen in the figure LSD technique is capable of measuring temperature distribution in the flow field while capturing characteristic structures. This application proves that, while developed technique, LSD, can easily be used for temperature or density measurements in compressible and reacting flows, it is also applicable in simultaneous measurement of velocity and temperature.

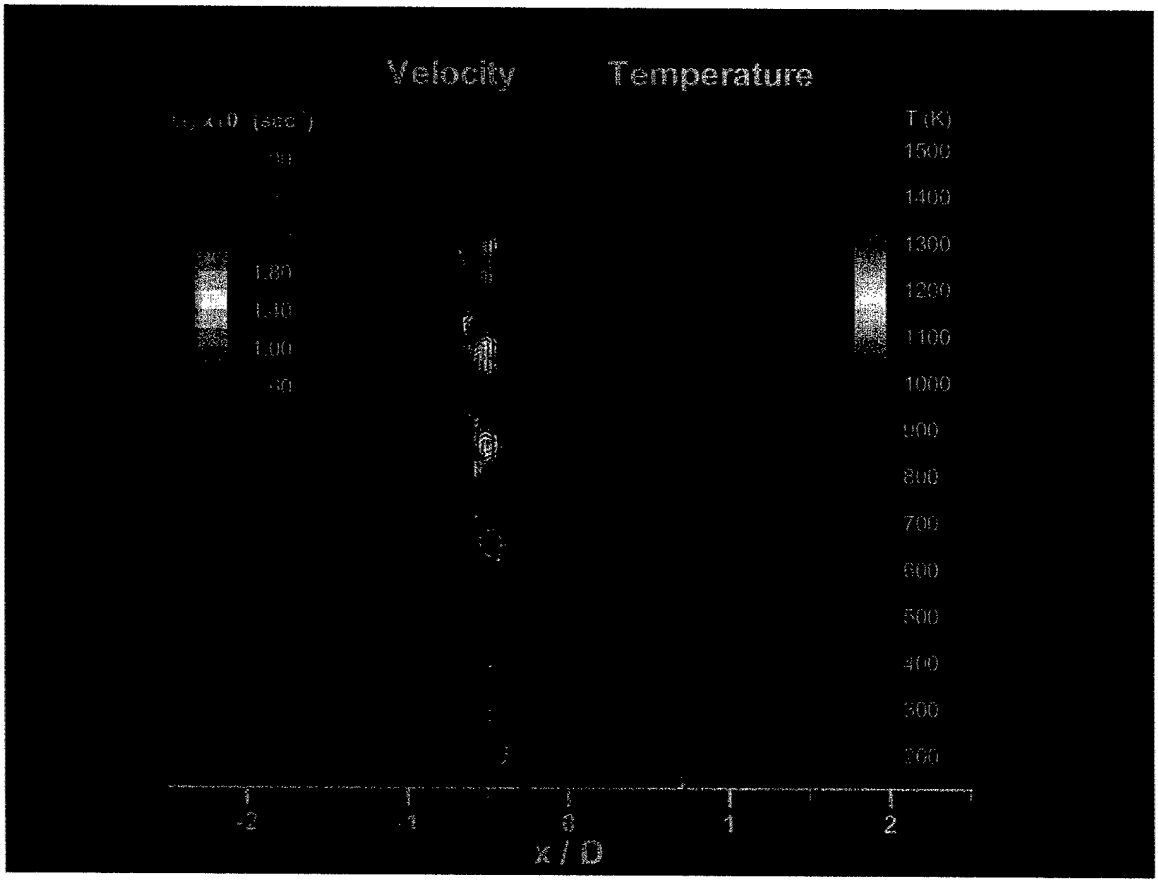

Figure 2.15. Combined temperature and velocity field from simultaneous temperature and velocity measurements.

3. RESULTS

The focus of this study is to introduce countercurrent shear layer control as a novel stabilization technique for premixed jet flames. Countercurrent control technique is based on the introduction of suction driven countercurrent flow around the periphery of the jet flame. This section of the report will present and discuss the experimental studies performed on the countercurrent controlled premixed propane-air jet flame.

3.1 Flame stability

To demonstrate the effect of countercurrent flow on the flame, a series of flow visualization pictures at different suction flow rates for the jet velocity, $U_1 = 5.5$ m/s and equivalence ratio, $\Phi = 2$ is shown in figure 3.1. The sequence shows the flame structure at the collar exit with increasing suction flow. It is seen that, the flame is stabilized by the application of the countercurrent flow. It is known that at high fuel concentrations a jet flame starts at a lifted location when it is ignited from the top (Wohl et al. 1949), which is the initial condition for the sequence shown in figure 3.1. It is depicted from figure 3.1 (a) that, at very low suction rates the flame is still lifted but its location is closer to nozzle exit. As the suction velocity increases, its effect is seen from single point attachment to the full anchoring of the flame. At suction velocity $U_2 = 1.06$ m/s the flame is firmly anchored at the nozzle exit and it is concluded that, the countercurrent control technique can be used in the stabilization of jet flames.

In the blow-off experiments flame was started with predetermined fuel amount at a high equivalence ratio to be able to get attached or lifted flame. Starting with high equivalence ratio at a fixed fuel flow rate results an initial condition with low jet velocity. Before applying countercurrent flow the jet velocity was increased until the flame lifts-off. The purpose of forcing the flame for lift off is the opposite effect of suction, i.e. disturbing effect of countercurrent flow on the stable flame. In the experiments it is noted that stabilizing effect of countercurrent flow is limited with the jet velocity, in other words, for a given jet velocity there is a maximum suction velocity that can be applied without disturbing the flame stability. This observation will be shown in shadowgraph pictures in the next section. When the suction is applied to lifted flame it is more likely to achieve attached stable flame. After igniting the mixture from top, suction driven countercurrent flow was applied around the periphery of the jet flame. For low suction velocities countercurrent flow rate was determined and set before the

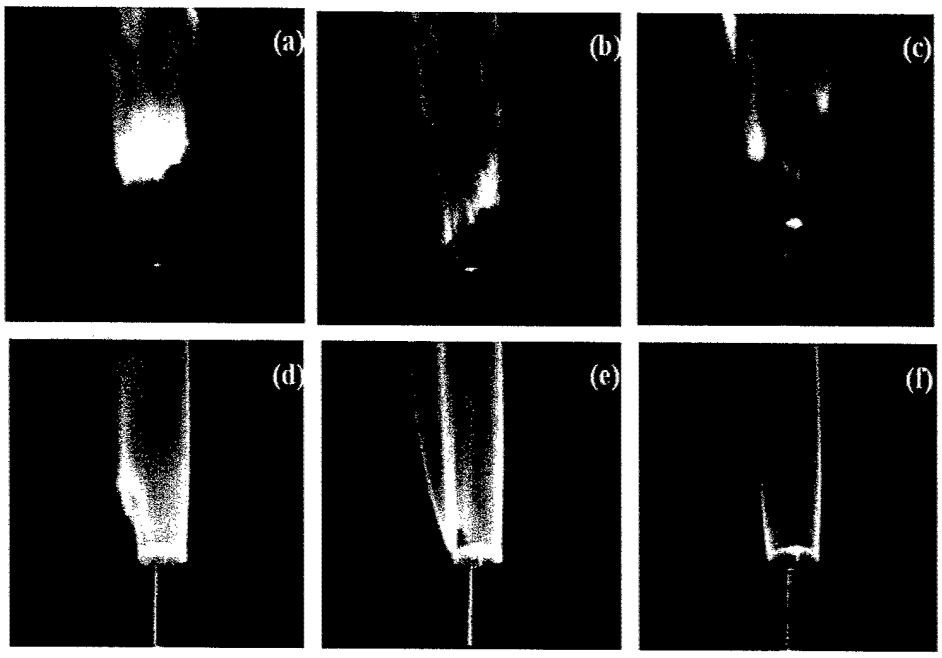

Figure 3.1. Flow visualization pictures showing the effect of increasing suction rate. $U_1 = 5.5$ m/s and $\Phi = 2$. (a) $U_2 = 0.2$m/s, (b) 0.4m/s, (c) 0.65m/s, (d) 0.83m/s, (e) 0.98m/s, (f) 1.06m/s.

experiment by fixing the control valve at the desired mass flow rate. For high countercurrent velocities, however, suction flow rate was increased gradually to avoid the disturbance. After applying the suction, air mass flow rate was increased in a controlled manner to prevent the sudden velocity changes and disturbances in the flame. The air mass flow rate at which flame extinguished was recorded as blow-off mass flow rate. The equivalence ratio was calculated from air and fuel flow rates which were measured at the instant of blow-off. The exit jet velocity is calculated by using the total mass flow rate of air and fuel, and the exit area of the nozzle burner. To show the effect of suction collar, and to compare the velocity increase with the application of countercurrent flow, the same experiments were performed for the cases of nozzle burner without the suction collar, which is called free jet, and nozzle burner with the suction collar but zero countercurrent velocity. Stability characteristic curve of the burner is given in figure 3.2 as a jet velocity U_1 versus equivalence ratio Φ plot. For the free jet flame unstable flame conditions are plotted as two separate curves. The first curve covers the range of equivalence ratio from 1.0 to 2.0. Up to equivalence ratio of 2.0 flame blows off (extinguishes)

when the jet exit velocity exceeds the flame propagation velocity. Above the equivalence ratio of 2.0, flame lifts off and it is stationary away from the nozzle exit. Since the purpose of this study is to attain attached flame by means of countercurrent control, lifted flame is considered as an unstable condition and shown with a separate curve. In figure 3.2 it is seen that at Φ=1.9 flame extinguishes when the jet velocity is increased to 3.5 m/s. This is the maximum jet velocity that the nozzle burner can operate at rich fuel-air mixtures. For very rich mixtures, Φ>2.0, flame lifts-off at a higher velocity with the increase of fuel amount. However the rise in the velocity is not a dramatic one when it is compared to the increase in equivalence ratio. Figure 3.2 also shows the stability characteristic of the nozzle burner with the presence of suction collar. In the experiments, it is observed that when the suction collar is present without the countercurrent flow, there is a remarkable increase in the blow-off velocity, particularly at the points with high equivalence ratio.

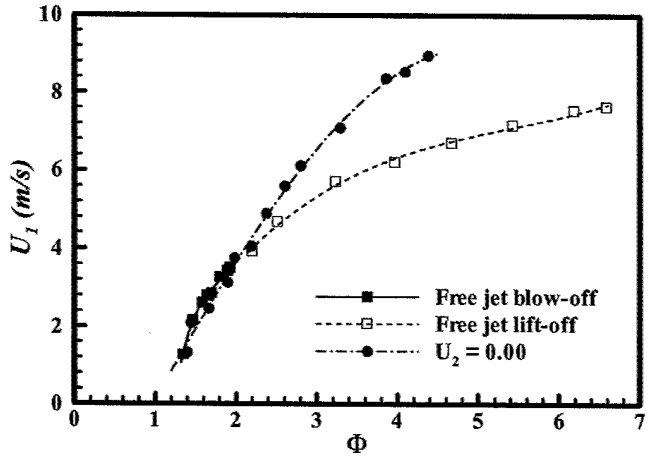

Figure 3.2 Nozzle burner stability characteristics with and without suction collar

From cold jet studies, it is known that the application of the countercurrent flow around the periphery of a jet changes the shear layer characteristics, which results in the variations in the velocity gradient. Since blow-off is explained with the velocity gradient variations in the jet flame, the consequences of the countercurrent flow can be seen as an increase or a decrease of the blow-off velocity. In figure 3.3 countercurrent effect on the blow-off limit of the rich premixed propane flame is presented as jet velocity, U_1, versus countercurrent velocity, U_2, plot

for different equivalence ratios. The experiment was limited to stoichiometric and rich premixed conditions, which are in the range of equivalence ratio of 1.0 to 2.0. In the figure it is seen that countercurrent flow has a remarkable effect on the blow-off velocity up to suction velocity of 3.0 m/s. At the countercurrent velocity of 3.0 m/s it is possible to obtain an attached stoichiometric premixed flame at the jet exit velocity of 20 m/s, which is an order of magnitude higher than the blow-off velocity achieved without suction. However, the increase in the stability limit is not directly proportional to the increase in suction velocity. In the case of stoichiometric flame, for the suction velocities higher than 3.0 m/s the, although blow-off velocity rises with the increasing suction velocity, the change is not a remarkable one and after the suction velocity of 4.0 m/s blow-off velocity remains constant. The same trend is also observed for higher equivalence ratios. When the effect of suction is discussed with respect to the variations in the equivalence ratio, it is seen that, for all equivalence ratios the blow-off velocity increases remarkably with an increasing countercurrent flow up to a certain suction velocity. In the investigation of countercurrent effect on the circular jets the velocity ratio is defined as $R = \Delta U / 2\overline{U}$, where $\Delta U = U_1 - U_2$ is the velocity difference and $\overline{U} = \frac{1}{2}(U_1 + U_2)$ is the average velocity of two streams. Strykowski and Niccum (1991) states the onset of global instability in a countercurrent controlled circular shear layer at the critical velocity ratio $R_{cr} = 1.32$ which is very close to convective/absolute instability transition velocity ratio, $R_t = 1.315$, calculated by Huerre and Monkewitz (1985). Based on these observations, the results of blow-off experiments are also presented as a velocity ratio versus suction velocity in figure 3.3b. When the results are examined with respect to critical velocity ratio, it is seen that, the upper limit of suction velocity range, in which significant blow-off velocity increase takes place, corresponds to countercurrent flow rate satisfying critical velocity ratio. Above the critical velocity ratio, R>1.32, the change in the blow-off velocity is insignificant. As it is seen in figure 3.3a, with the increase of equivalence ratio blow-off velocity curves are getting closer to each other.

Observations on the blow-off velocity change with the equivalence ratio and the suction velocity lead us to the conclusion that there should be an upper and a lower limit in the application of countercurrent flow as a control technique. The lower limit of the stability condition is defined as the minimum countercurrent flow necessary to attain attached flame at a fixed fuel-air ratio, upper limit is the maximum suction that can be applied without causing any

disturbance in an attached flame. The results of stability limit experiments are presented in figure 3.4. At each point on the figure flame was started with a fixed fuel-air ratio and, for the cases at which jet velocity exceeds the flame propagation velocity, flame was anchored by applying the countercurrent flow. To determine the lower limit of the stable flame suction flow rate was decreased in a controlled manner to avoid the sudden condition changes at the nozzle exit. The suction velocity at which flame was detached from the nozzle was recorded as the lower stability limit of the chosen fuel-air ratio. The same procedure was applied for upper stability limit by increasing the countercurrent flow rate. As it is mentioned before, there is a maximum suction amount for a given jet velocity that can be applied without disturbing the flame and this is the upper stability limit of a countercurrent controlled premixed jet flame. In figure 3.4 results are shown as velocity ratio versus equivalence ratio plot, which shows the boundaries of the stable flame operation in (R,Φ) parameter space. As it is seen in the plot, when the suction velocity is introduced in the velocity ratio, stability limits of the flame can be represented by upper limit and lower limit curves. At velocity ratios lower than lower stability limit, flame blows-off because of insufficient countercurrent flow. However in the region above the upper stability curve, flame lifts-off from the nozzle burner. In the next section shadowgraph visualization of premixed jet flame with varying suction flow will be shown to demonstrate the effect of excess countercurrent flow.

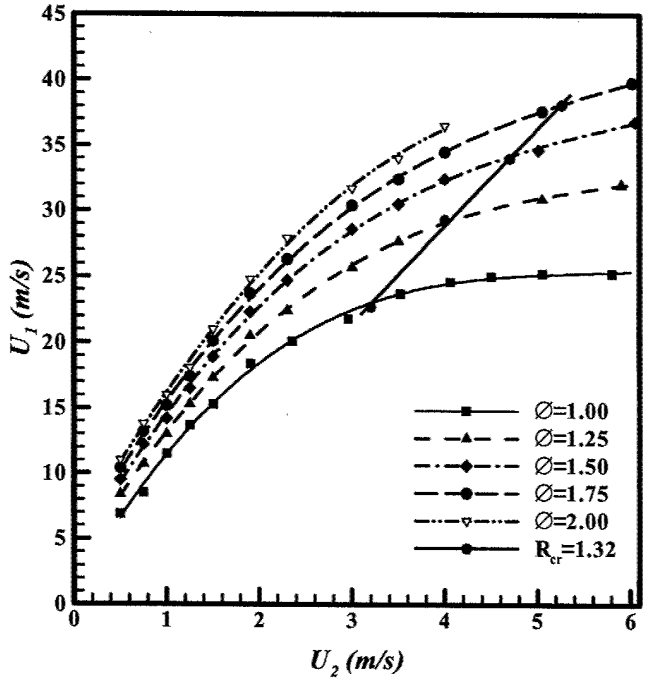

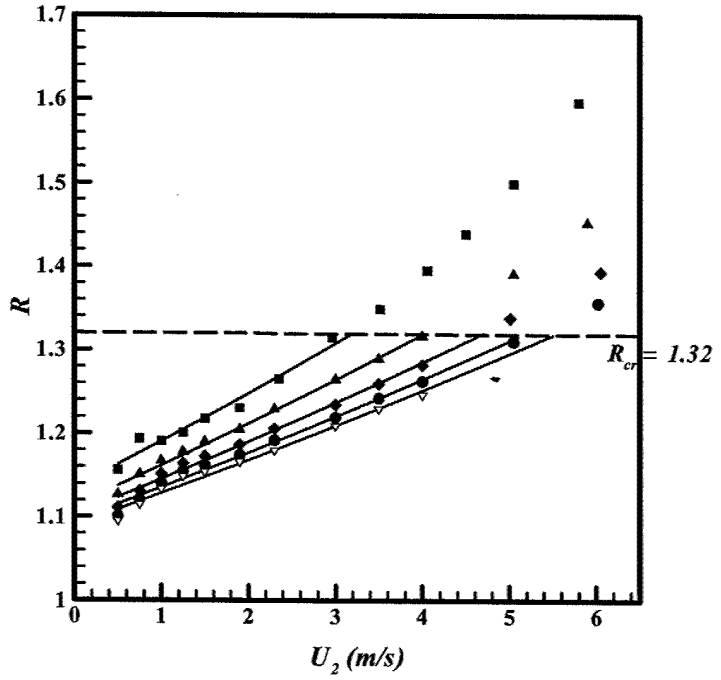

Figure 3.3 a) Blow-off limit of countercurrent controlled jet flame, b)Blow-off limits as a velocity ratio R versus suction velocity U_2 plot.

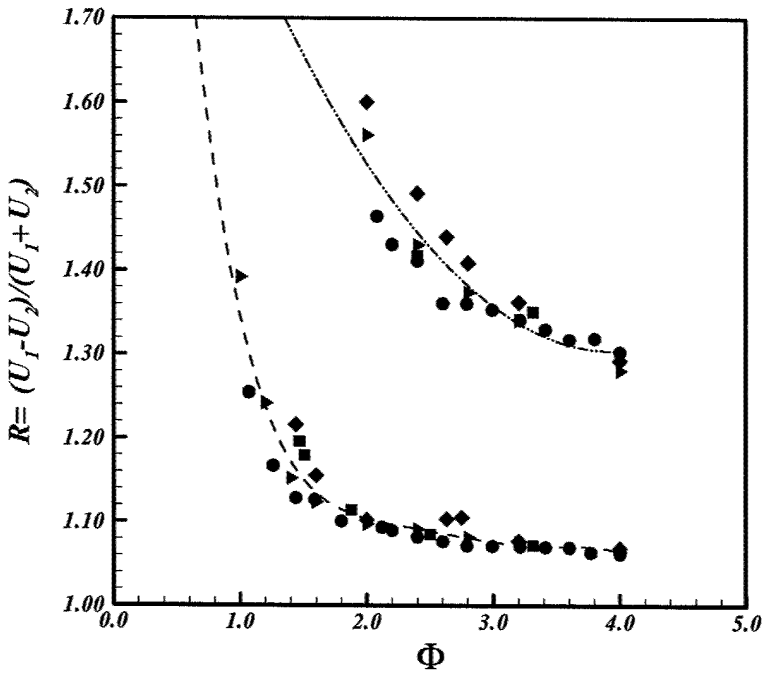

Figure 3.4 Stability limits of a countercurrent stabilized jet flame.

3.2 Countercurrent effect on the flow structure

As it is mentioned before the effect of countercurrent flow on the flame can be disturbing at a certain suction velocity. To observe the changes in the flow structure of the premixed jet, flame shadowgraph visualizations were performed at different suction velocities including the zero suction velocity. During the experiments flame was started with a high air to fuel ratio as an attached flame. While the velocity of the jet and the fuel flow rate were being kept constant, suction flow rate was increased in each case until the flame was disturbed. Yule et al. (1981) presented that in transitional flames Kelvin-Helmholtz instabilities in the flames are accompanied by combustion driven instabilities. They investigated the flame-flow interaction for a wide range of equivalence ratio values from ∞ (diffusion flame) to 1.5. They reported that for the flame $\Phi = 10.4$ and $Re = 10^4$, flow structure is made of fast moving inner eddies, that are formed from the wave instabilities as an interaction of hot burned gases and the cold fuel-air mixture, and slowly proceeding outer eddies. In their visualization study a laminar cylindrical flame region was defined at the exit of the nozzle up to 1.3D (D is the nozzle diameter at the

exit) in the axial direction, which is the onset location of visible inner instability. In this study shadowgraph visualizations were made at different exit velocities and equivalence ratios. Figure 3.5 shows visualization pictures of a rich premixed jet flame at the jet velocity of 5.8 m/s and the equivalence ratio of 3.25 with $Re = 3.6x10^3$. As it is mentioned before the burner nozzle is surrounded by a suction color with the height of 1.0D that avoids the observation of nozzle exit. But when figure 3.5 is examined it is seen that the inner flow structure at the tip of the suction collar, at x = 1.0D, changes with an increasing suction velocity. In the figure, instantaneous images of the flow are arranged from zero suction velocity to maximum suction velocity. Originally, i.e. the case without suction, flow field is formed of bigger vortices appearing at the tip of the suction collar. When the countercurrent flow is introduced the size of the vortices get smaller in the first 5.0D of the flow with the increasing velocity ratio. The change in the flow structure for R>1.32 is more distinctive than the changes take place at lower velocity ratios. As it is seen in the figure, at the condition of R=1.39, the formation of the individual vortices is appears much further downstream from the nozzle exit. From images it is clear that although the vortex shedding frequency is constant, increased suction reduces the vortex growth rate. The picture at R = 1.96 suggests that increased suction flow introduces different modes of instability to the flow. While at lower R values instability of the cold fuel-air mixture column can be described as axisymmetric, at R = 1.96 cold mixture column shows sinuous oscillations, which turns into helical mode of the instability with the further increase of the velocity ratio to R = 1.99. The onset of the helical mode appears to correspond to the conditions of the upper limit of the stability in Figure 3.4.

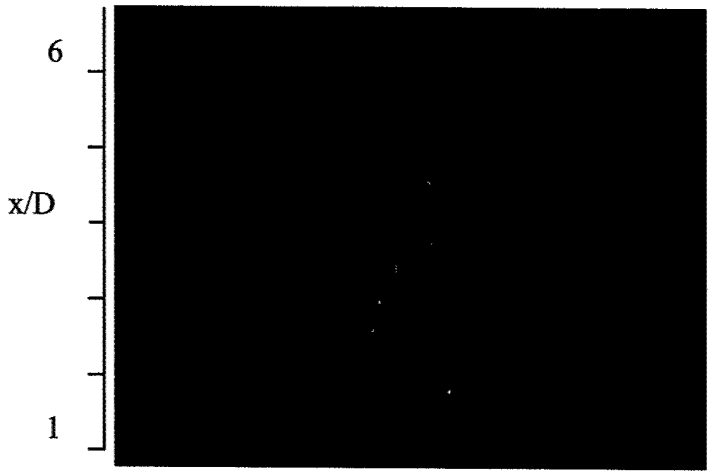

a) U_2= 0.0 m/s, R = 1.0

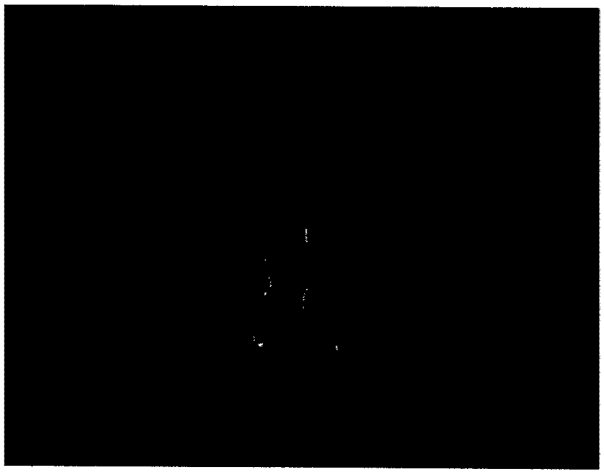

b) U_2= 0.26 m/s, R = 1.09

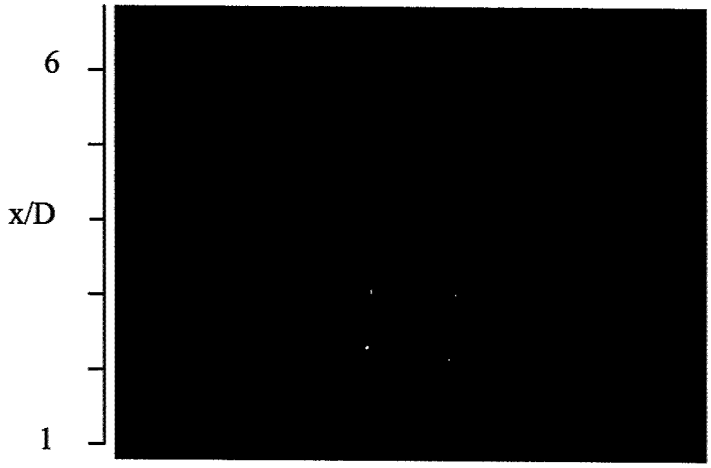

c) U_2= 0.56 m/s, R = 1.21

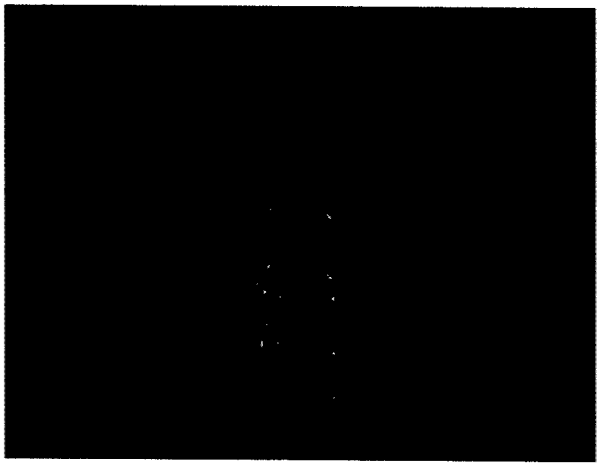

d) U_2= 0.71 m/s, R = 1.28

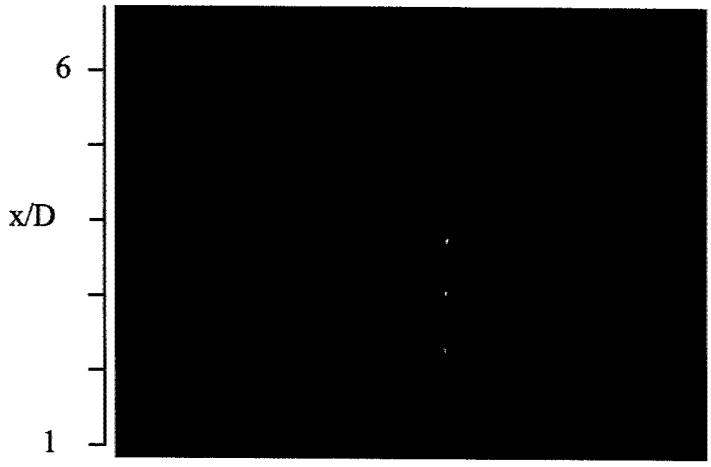

e) U_2= 0.94 m/s, R = 1.39

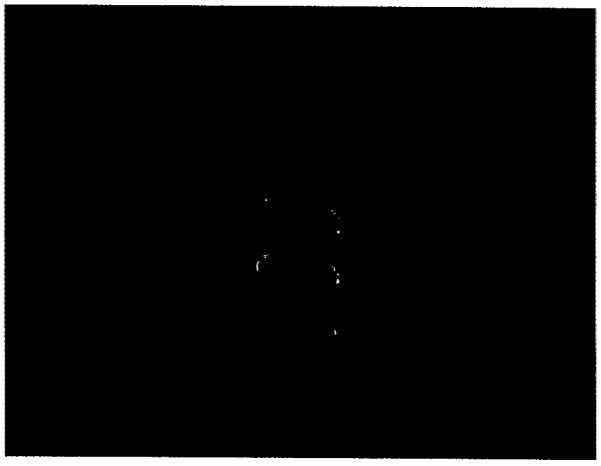

f) U_2= 1.10 m/s, R = 1.47

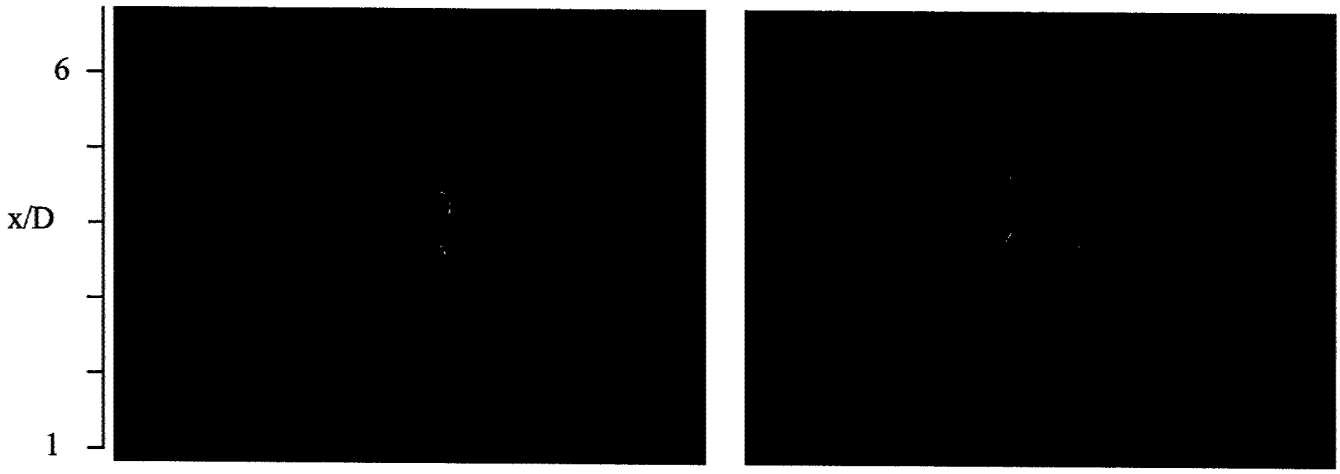

g) U_2= 1.27 m/s, R = 1.56

h) U_2= 1.52 m/s, R = 1.71

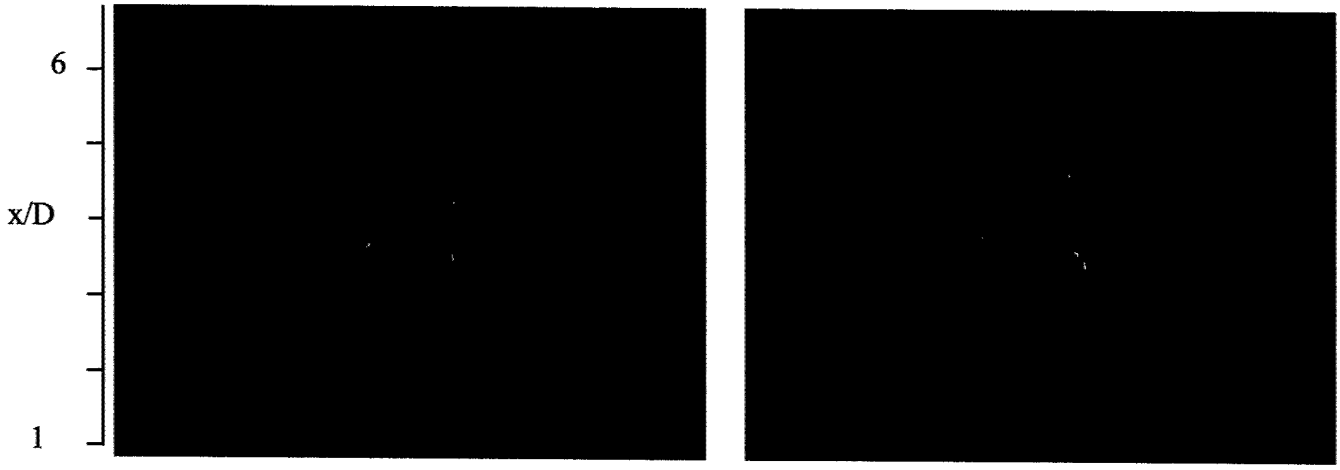

i) U_2= 1.77 m/s, R = 1.88

j) U_2= 1.88 m/s, R = 1.96

k) U_2= 1.92 m/s, R = 1.99

3.3 Velocity field measurements by means of PIV

In this section the characteristics of the turbulent premixed flame will be presented with the data collected by means of PIV measurements. First experiments aimed to observe the countercurrent flow at the lip of the suction collar to verify that the source of the countercurrent flow is ambient air, not the fuel-air mixture. Figure 3.6, which is a result of close-up PIV measurements at a suction velocity of 1.5 m/s, shows streamlines of the countercurrent flow are originated from the surrounding air. It is known that blow off velocity for a flame is predetermined by the strain rate distribution in the flow, i.e. the magnitude of the commonly used strain rate S_{xy}, can provide an indication of flame extinction. Strain rate is defined as $S_{xy} = (\partial u/\partial y + \partial v/\partial x)/2$ where u and v are the axial and the transverse velocity components respectively. To present the suction effect on the shear layer, in figure 3.7 typical instantaneous velocity fields superimposed with strain rate fields and strain rates of a stable flame without suction is compared to strain rates of attached flames at a higher jet velocity with the application of two different suction velocities while in all three cases equivalence ratio is constant. Figure 3.7(a) shows a stable flame without any countercurrent flow while the suction collar is present and the jet velocity is 5 m/s at the equivalence ratio $\Phi = 1.8$. In figure 3.3 it is depicted that, at the equivalence ratio of 1.8, blow off velocity changes in the range of 10 - 35 m/s depending on the countercurrent flow rate. Since with the application of suction a stable flame is attained at a higher jet velocity the comparison is made between the stable flame at 5 m/s without suction and a countercurrent stabilized flame at 11.5 m/s to demonstrate the change in the strain rates. In figure 3.7(a) the magnitude of the maximum strain rate S_{xy} observed for a stable flame without the countercurrent flow is around 650 s^{-1}, a value close to that found in a laminar premixed flame at a lower Reynolds number of 940 (Mungal et al. 1995). The stable flame obtained with suction shows a significant increase in strain rate as shown in figure 3.7(b,c) with the maximum value of 1650 s^{-1}, which is less than the extinction stretch rate of about 1900 s^{-1} measured by Law (1988). From PIV experiments it is concluded that countercurrent flow stabilizes the flame by reducing strain rates below the extinction limit at high velocities.

Besides investigating the effect of suction on the shear layer, PIV experiments were made to observe the changes in the flow structure of the premixed flame very close to blow off velocities. In these experiments stereoscopic PIV was used to determine the out of plane fluctuating velocity component. Measurement conditions were chosen on the blow off velocity curve, shown

in figure 3.3(a), at $\Phi = 1.0$. Results of these experiments are presented in figure 3.8 as turbulent kinetic energy plots. As it is seen in the figure, as the suction velocity increases the potential core of the flame, which is the region where cold fuel-air mixture is present, gets longer and turbulent kinetic energy increases in the shear layer.

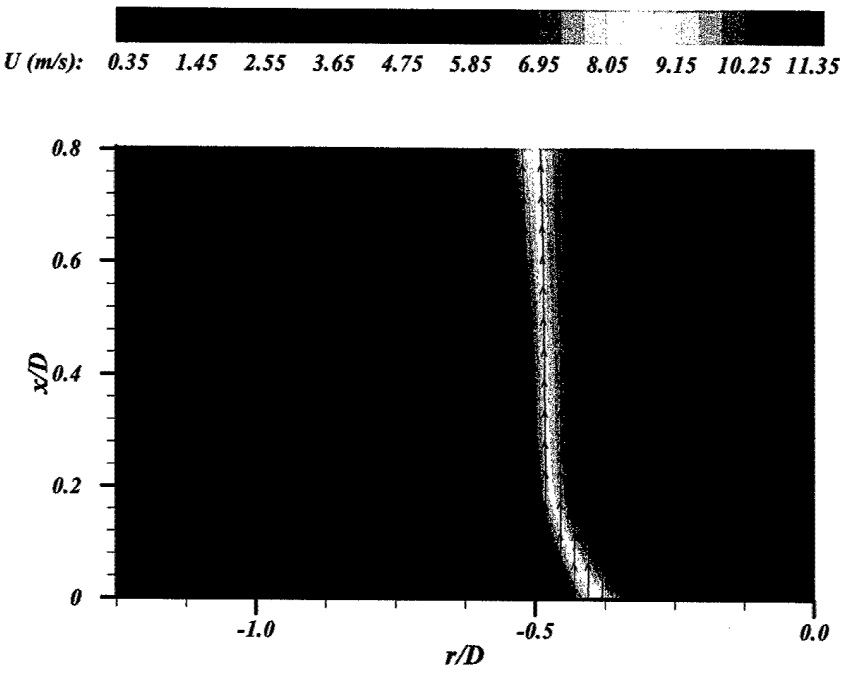

Figure 3.6. Stream line pattern at the nozzle exit

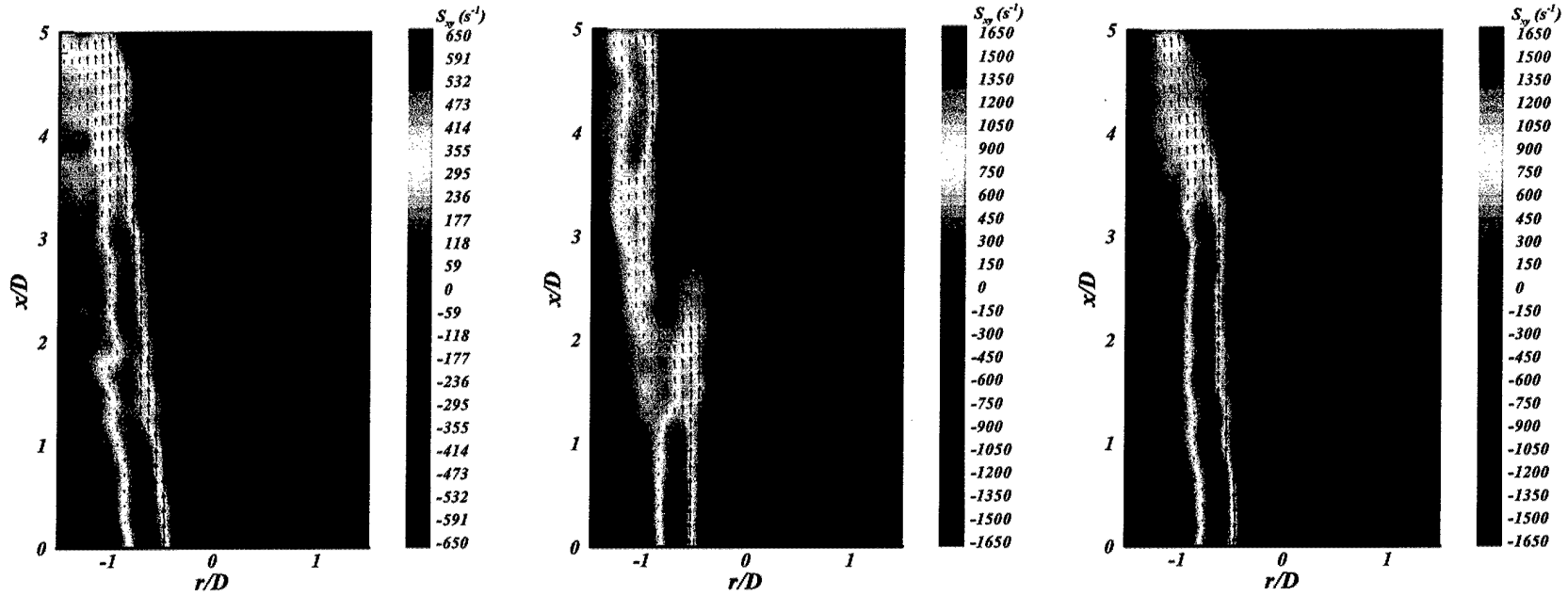

a) U_1=5 m/s, U_2=0, Φ=1.8

b) U_1=11.5 m/s, U_2=1.0, Φ=1.8

c) U_1=11.5 m/s, U_2=1.5, Φ=1.8

Figure 3.7. Instantaneous strain and velocity fields at different suction velocities.

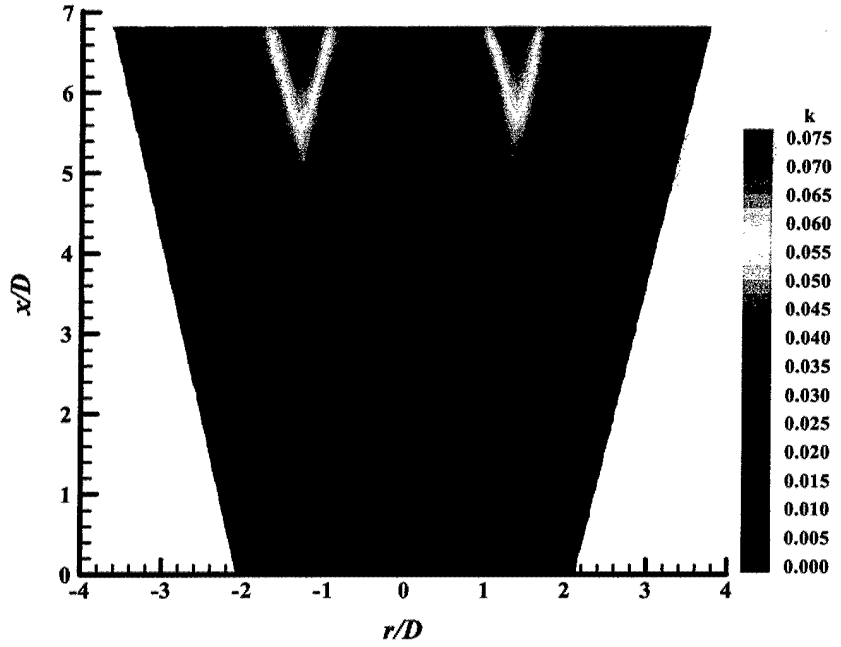

a) U_1=11.0 m/s, U_2=1.0, Φ=1.0

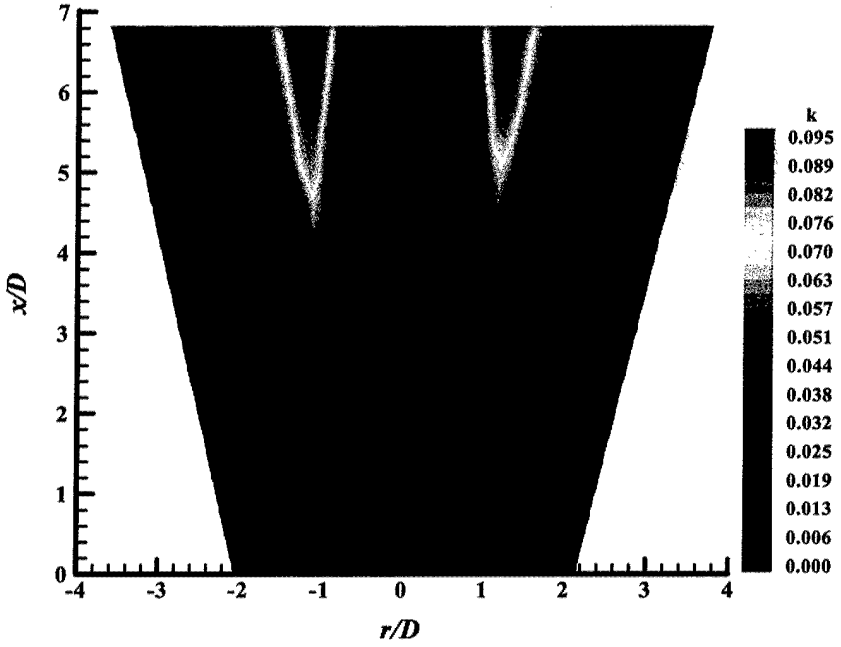

b) U_1=16.0 m/s, U_2=1.85, Φ=1.0

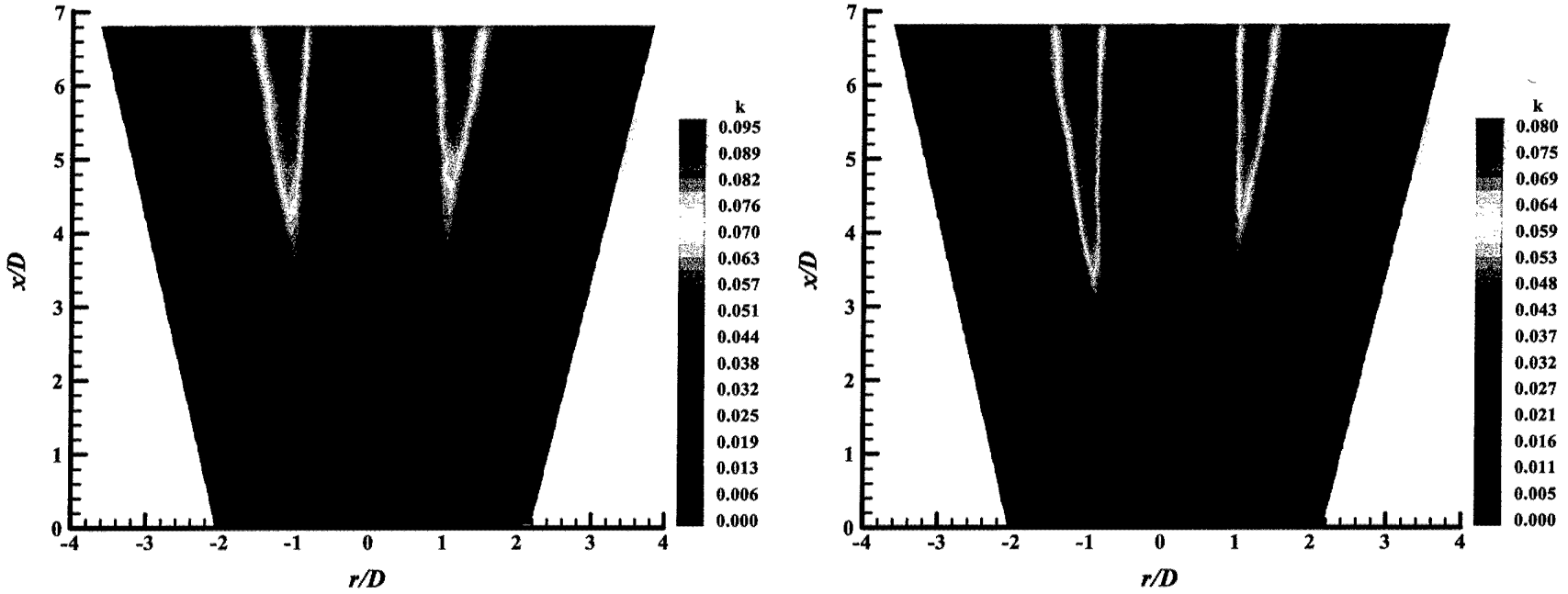

c) U_1=18.0 m/s, U_2=2.4, Φ=1.0

d) U_1=20.0 m/s, U_2=3.5, Φ=1.0

Figure 3.8. Turbulent kinetic energy distribution

4. SUMMARY

Countercurrent shear layer control was applied as a novel flame stabilization technique for premixed jet flames. The countercurrent is applied around the periphery of the jet within the first one diameter of the nozzle exit. With the application of suction an order of magnitude increase in the blow off velocity was obtained. It is known that flame stability is determined by shear layer strain rates and the mixing. From PIV measurements it is seen that application of suction reduces the strain rates along with turbulent kinetic energy increase in the shear layer.

In the experiments stereoscopic PIV was successfully applied to velocity field measurements in a premixed jet flame. Additionally, an optical temperature measurement technique, called Laser Speckle Displacement (LSD), was developed for the measurement of instantaneous temperature fields in an axisymmetric jet flame. The basic principle of the technique is known as speckle photography and it has been worked on for three decades. In previous applications of the technique, refractive index gradients in axial direction were assumed negligible. However with the new calculation algorithm introduced in this study it was shown that axial refractive index gradients are also important in the measurement of temperature field. It is demonstrated that LSD and PIV techniques can be used together for simultaneous velocity and temperature field measurements in an axisymmetric jet flame.

REFERENCES

Alkislar, M.B., Lourenco,L., and Krothapalli, A.(2000) *Stereoscopic PIV measurements of a screeching supersonic jet,* J. Visualization, 3-2: .

Alkislar, M.B.(2001) *Flow field measurements in a screeching rectangular jet,* Ph.D. Thesis.

Born, M., and Wolf, E. (1980) *Principles of optics*, Oxford: Pergamon Press.

Cremers, C.J. and Birkebak R.C. (1966) *Application of the Abel integral equation to spectrographic data,* Applied Optics, 5-6: 1057-1064.

Debrus, S., Francon, M., Grover, C.P., May, M., and Robin, M.L. (1972) *Ground glass differential interferometer,* Applied Optics, 11-4: 853-857.

Erbeck, R. and Merzkirch, W. (1988) *Speckle photographic measurement of turbulence in an air stream with fluctuating temperature,* Experiments in Fluids, 6: 89-93.

Farrell, P.V. and Hofeldt, D.L. (1984) *Temperature measurement in gases using speckle photography*, Applied Optics, 27–7: 1055-1059.

Fomin, N.A. (1998) *Speckle photography for fluid mechanics measurements*, New York : Springer.

Fomin, N., Lavinskaja, E., Merzkirch, W., and Vitkin, D. (1999) *Speckle photography applied to statistical analysis of turbulence,* Optics & Laser Technology, 31: 13-22.

Francon, M. (1979) *Laser speckle and applications in optics,* New York: Academic Press.

Gardiner, W.C., Hidaka, Y., and Tanzawa, T. (1981) *Refractivity of combustion gases,* Combustion and Flame, 40: 213-219.

Gebhard, P., Klas, J., and Strube, G. (1994) *Optical measurements: techniques and applications*,(Ed. Mayinger, F.) pp5-9, Berlin; New York : Springer-Verlag.

Huerre, P., and Monkewitz, P.A. (1985) *Absolute and convective instabilities in free shear layers,* J. Fluid. Mech., 159: 151-168.

Keller, J. and Merzkirch, W. (1990) *Interaction of a normal shock wave with a compressible turbulent flow,* Experiments in Fluids, 8: 241-248.

Kopf, U. (1972) *Application of speckling for measuring the deflection of laser light by phase objects,* Optics Communications, 5-5: 347-350.

Law, C. K. (1988) *Dynamics of stretched flames*, Twenty-second Symposium (International) on Combustion, The Combustion Institute, Pittsburgh: 1381-1402.

Lourenco, L., and Krothapalli, A. (2000) *True resolution PIV: A mesh-free second-order accurate algorithm*, Proceedings of the 10th International Symposium on Applications of Laser Techniques in Fluid Mechanics, Lisbon, Portugal.

Mungal, M. G., Lourenco, L. M., and Krothapalli, A. (1995) *Instantaneous velocity measurements in a laminar and turbulent premixed flames using on-line PIV*, Combust. Sci. and Tech., 106: 239-265.

Rubinstein, R. and Greenberg, P.S. (1994) *Rapid inversion of angular deflection data for certain axisymmetric refractive index distributions,* Applied Optics, 33-7: 1141-1144.

Shakher, C., Daniel, A.J.P, and Nirala, A.K.(1994) *Temperature profile measurement of axisymmetric gaseous flames using speckle photography, speckle shearing interferometry, and Talbot interferometry,* Optical Engineering, 33-6: 1983-1988.

Strykowski, P. J. and Niccum, D.L. (1991) *The stability of countercurrent mixing layers in circular jets,* J. Fluid. Mech., 227: 309-343.

Strykowski, P. J. and Niccum, D.L. (1992) *The influence of velocity and density ratio on the dynamics of spatially developing mixing layers,* Phys. of Fluids, 4-4: 770-781.

Strykowski, P. J., and Wilcoxon, R. K. (1993) *Mixing enhancement due to global oscillations in jets with annular counterflow*, AIAA J., 31-4: 564-570.

Strykowski, P. J., and Krothapalli, A. (1993) *The countercurrent mixing layer: strategies for shear-layer control*, AIAA Shear flow conference, Orlando, paper No.93-3260.

Wernekinck, U., and Merzkirch, W. (1987) *Speckle photography of spatially extended refractive index fields*, Applied Optics, 26 –1: 31-32.

Williams, F.A. (1985) *Combustion theory*, Menlo Park, California: Benjamin/Cummings Pub. Co.

Wohl, K., Kapp, N. M., and Gazley, C. (1949) *The stability of open flames*, Third Symposium on Combustion, Flame and Explosion Phenomena, pp. 3-21, The Combustion Institute, Pittsburg.

Yule, A.J., Chigier, N.A., Ralph, S., Boulderstone, R., and Ventura, J. (1981) *Combustion - transition interaction in a jet flame,* AIAA J., 19-6: 752-760.